

AD-A174 171 COMPUTER SIMULATION AND EXPERIMENTAL VALIDATION OF A
DYNAMIC MODEL (EQUIV (U) NAVAL POSTGRADUATE SCHOOL
MONTEREY CA R P PETROKA JUN 86

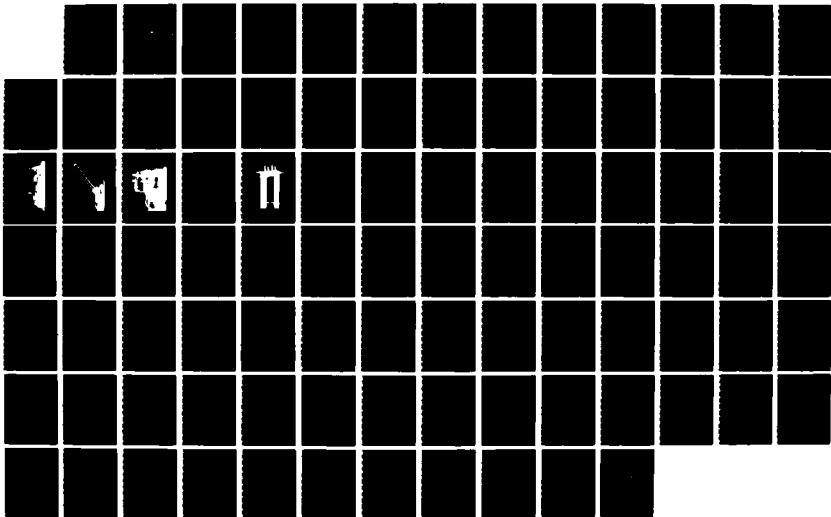
AD-A174 171 COMPUTER SIMULATION AND EXPERIMENTAL VALIDATION OF A
DYNAMIC MODEL (EQUIV (U) NAVAL POSTGRADUATE SCHOOL
MONTEREY CA R P PETROKA JUN 86

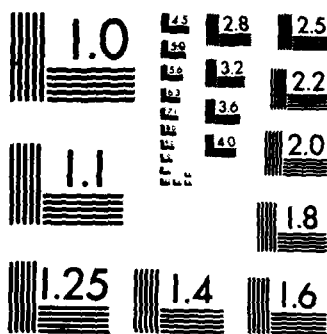
1/1

UNCLASSIFIED

F/G 9/2

NL





XEROCOPY RESOLUTION TEST CHART
NATIONAL BUREAU OF STANDARDS-1963-A

2

AD-A174 171

NAVAL POSTGRADUATE SCHOOL

Monterey, California



DTIC
ELECTE
NOV 20 1986
S B

THESIS

COMPUTER SIMULATION AND EXPERIMENTAL
VALIDATION OF A DYNAMIC MODEL
(EQUIVALENT RIGID LINK SYSTEM) ON
A SINGLE-LINK FLEXIBLE MANIPULATOR

by

Robert P. Petroka

June 1986

Thesis Advisor:

Liang-Wey Chang

Approved for public release; distribution is unlimited.

DTIC FILE COPY


86 11 19 007

AD-2174171

REPORT DOCUMENTATION PAGE

1a REPORT SECURITY CLASSIFICATION UNCLASSIFIED		1b. RESTRICTIVE MARKINGS													
2a SECURITY CLASSIFICATION AUTHORITY		3 DISTRIBUTION/AVAILABILITY OF REPORT Approved for public release; distribution is unlimited.													
2b DECLASSIFICATION/DOWNGRADING SCHEDULE		5 MONITORING ORGANIZATION REPORT NUMBER(S)													
4 PERFORMING ORGANIZATION REPORT NUMBER(S)		7a. NAME OF MONITORING ORGANIZATION Naval Postgraduate School													
6a. NAME OF PERFORMING ORGANIZATION Naval Postgraduate School	6b OFFICE SYMBOL (If applicable) 69	7b. ADDRESS (City, State, and ZIP Code) Monterey, California 93943-5000													
6c ADDRESS (City, State, and ZIP Code) Monterey, California 93943-5000	8b. OFFICE SYMBOL (If applicable)	9. PROCUREMENT INSTRUMENT IDENTIFICATION NUMBER													
3a NAME OF FUNDING/SPONSORING ORGANIZATION	8c. ADDRESS (City, State, and ZIP Code)	10 SOURCE OF FUNDING NUMBERS <table border="1"><tr><td>PROGRAM ELEMENT NO</td><td>PROJECT NO</td><td>TASK NO</td><td>WORK UNIT ACCESSION NO</td></tr></table>		PROGRAM ELEMENT NO	PROJECT NO	TASK NO	WORK UNIT ACCESSION NO								
PROGRAM ELEMENT NO	PROJECT NO	TASK NO	WORK UNIT ACCESSION NO												
11 TITLE (Include Security Classification) COMPUTER SIMULATION AND EXPERIMENTAL VALIDATION OF A DYNAMIC MODEL (EQUIVALENT RIGID LINK SYSTEM) ON A SINGLE-LINK FLEXIBLE MANIPULATOR															
12 PERSONAL AUTHOR(S) Petroka, Robert P.															
13a TYPE OF REPORT Master's Thesis	13b TIME COVERED FROM _____ TO _____	14 DATE OF REPORT (Year, Month, Day) 1986 June	15 PAGE COUNT 92												
16 SUPPLEMENTARY NOTATION															
COSATI CODES <table border="1"><tr><td>FIELD</td><td>GROUP</td><td>SUB-GROUP</td></tr><tr><td></td><td></td><td></td></tr><tr><td></td><td></td><td></td></tr><tr><td></td><td></td><td></td></tr></table>		FIELD	GROUP	SUB-GROUP										18 SUBJECT TERMS (Continue on reverse if necessary and identify by block number) Flexible Manipulator, Manipulator, Robotics, Dynamic Model, Robot	
FIELD	GROUP	SUB-GROUP													
19 ABSTRACT (Continue on reverse if necessary and identify by block number) <p>Flexibility effects on robot manipulator design and control are typically ignored which is justified when large, bulky robotic mechanisms are moved at slow speeds. However, when increased speed and improved accuracy is desired in robot system performance it is necessary to consider flexible manipulators. This project simulates the motion of a single-link, flexible manipulator using the Equivalent Rigid Link</p>															
20 DISTRIBUTION/AVAILABILITY OF ABSTRACT <input type="checkbox"/> UNCLASSIFIED/UNLIMITED <input type="checkbox"/> SAME AS RPT <input type="checkbox"/> DTIC USERS		21 ABSTRACT SECURITY CLASSIFICATION UNCLASSIFIED													
22a NAME OF RESPONSIBLE INDIVIDUAL Liang-Wey Chang		22b TELEPHONE (Include Area Code) 408-649-1036	22c OFFICE SYMBOL 69CK												

System dynamic model and experimentally validates the computer simulation results. Validation of the flexible manipulator dynamic model is necessary to ensure confidence of the model for use in future design and control applications of flexible manipulators.



Approved for public release; distribution is unlimited.

COMPUTER SIMULATION AND EXPERIMENTAL VALIDATION
OF A DYNAMIC MODEL (EQUIVALENT RIGID LINK SYSTEM)
ON A SINGLE-LINK FLEXIBLE MANIPULATOR

by

Robert P. Petroka
Lieutenant Commander, United States Navy
B.S., United States Naval Academy, 1976

Submitted in partial fulfillment of the
requirements for the degrees of

MASTER OF SCIENCE IN MECHANICAL ENGINEERING

and

MECHANICAL ENGINEER

from the

NAVAL POSTGRADUATE SCHOOL
June 1986

Author:

Robert P. Petroka

Robert P. Petroka

Approved by:

Ling Wey Chang

L.W. Chang, Thesis Advisor

David Smith

D.L. Smith, Second Reader

Paul J. Marto
Paul J. Marto, Chairman,
Department of Mechanical Engineering

John N. Dyer
John N. Dyer,
Dean of Science and Engineering

ABSTRACT

Flexibility effects on robot manipulator design and control are typically ignored which is justified when large, bulky robotic mechanisms are moved at slow speeds. However, when increased speed and improved accuracy is desired in robot system performance it is necessary to consider flexible manipulators. This project simulates the motion of a single-link, flexible manipulator using the Equivalent Rigid Link System dynamic model and experimentally validates the computer simulation results. Validation of the flexible manipulator dynamic model is necessary to ensure confidence of the model for use in future design and control applications of flexible manipulators.

TABLE OF CONTENTS

I.	INTRODUCTION -----	7
II.	THEORETICAL APPROACH -----	15
III.	EXPERIMENTAL APPROACH -----	22
IV.	RESULTS -----	34
V.	CONTROL OF FLEXIBLE MANIPULATORS -----	50
VI.	CONCLUSIONS -----	56
VII.	RECOMMENDATIONS -----	59
APPENDIX A.	DERIVATION OF THE EQUATIONS OF MOTION FOR THE EXPERIMENTAL, SINGLE-LINK, FLEXIBLE ARM -----	61
APPENDIX B..	LISTING OF THE FORTRAN CODING UTILIZED IN SOLVING THE DYNAMIC EQUATIONS OF MOTION FOR THE EXPERIMENTAL, SINGLE-LINK, FLEXIBLE ARM -----	71
APPENDIX C.	DERIVATION OF THE SHAPE FUNCTION MATRIX AND THE NODAL DISPLACEMENT VECTOR -----	82
APPENDIX D.	LINEARIZATION, STATE SPACE REPRESENTATION, AND OPTIMAL CONTROLLER DESIGN OF SINGLE- LINK DYNAMIC EQUATIONS (ERLS) -----	85
	LIST OF REFERENCES -----	88
	INITIAL DISTRIBUTION LIST -----	90



Accession for	
NTIS	<input checked="" type="checkbox"/>
DTIC	<input type="checkbox"/>
Unannounced	<input type="checkbox"/>
Just	<input type="checkbox"/>
By	
Dist	
Approved for	
Dist	
A-1	

ACKNOWLEDGEMENT

I wish to express my sincerest gratitude to my advisor, Professor Liang-Wey Chang, for his unselfish giving of his time and knowledge in support of this research. His friendship and his commitment as an educator to impart practicality to engineering theory will always be remembered. Appreciation is also extended to Professors David Smith and Robert Nunn for their timely guidance in the course of this research.

I also want to thank my wife, Donna, for her encouragement during this past year and for her interest and enthusiasm in my research project.

I finally want to thank my Lord and Savior, Jesus Christ, for the wisdom, strength, and peace He gave me this past year enabling me to complete this thesis research.

I. INTRODUCTION

The desire to design, build, and operate a lightweight, long-reach manipulator for NASA space shuttle usage was a prime impetus for generating interest in the flexibility effects of robotic arms [Ref. 1: pp. 3, 9]. Interest in improving productivity in automated manufacturing plants through increased speed and accuracy have additionally sparked a desire to further investigate flexibility effects in mechanical devices [Ref. 2: pp. 1, 2]. The design, construction, and operation of a flexible robotic manipulator arm has many attractive features. In the past the manipulator was assumed being composed of rigid links and dictated that the link design be large members, both in cross-sectional area and weight. The flexible arm would require minimal material and consequently would have less weight and bulk than conventional rigid-arm robots. With a smaller, lighter weight manipulator, less power would be needed to move the arm which could mean use of smaller actuators. Arm speed movement would increase if the actuator size is not reduced. A smaller, lighter weight manipulator would require less foundation mounting strength and rigidity requirements. The reduced foundation mounting requirements coupled to the less material required for the arm construction would translate to a lower overall cost to build a flexible-arm robot compared

to a rigid-arm robot. The reduced mass of the flexible-arm robot would cause less damage if inadvertent collision occurred and would be consequently safer to operate compared to a rigid-arm robot. Finally, the reduced weight of the flexible-arm robot would allow for easy transportability [Ref. 3: p. 1209].

The preceding discussion of the advantages of utilizing flexible-arm robots points to their tremendous potential for application in industry, in the military, and in space. In spite of these advantages for utilizing flexible-arm robots, until recently there has been a reluctance to investigate the design and control of flexible manipulator arms. One reason for this reluctance is the degradation of the end-effector positioning accuracy due to the increased deformation of the lightweight, flexible arm. Also, the increased vibration of the flexible arm causes a significant control problem when coupled with the large-scale translational and/or rotational motion of the robot [Ref. 3: p. 1209]. This control problem arises due to the reduced bandwidth of the flexible manipulator system and the consequent limitation on values of gain in the control design. The reduced bandwidth is the result of the lower fundamental frequency inherent in a flexible manipulator system compared to a rigid system. In order to benefit from the advantages of lightweight, flexible manipulators it is necessary to implement a control design capable of achieving end-effector positioning accuracy and stable control.

Extensive research began in the early 1980's into the design and control aspects of a flexible manipulator arm. Information on the dynamic response and the natural frequencies of the flexible manipulator arm is useful to the designer in predicting deformations and stress levels. An accurate dynamic model including flexibility allows for simulation studies by the designer enabling him to extract his required information. An accurate dynamic model including flexibility is also necessary for any controller design which is to subsequently control a flexible manipulator [Ref. 2: pp. 2, 3]. An integral, essential part of improving the accuracy and stability problems associated with flexible manipulator arms is, therefore, the development of an accurate, dynamic model of the flexible arm. There are several approaches to the development of a flexible structure dynamic model in the literature, some of which are reviewed below.

Until recently, the approach to modeling robotic mechanisms assumed a rigid structure. The motion consequently described by these models included only the large, rigid-body motion, hereafter referred to as large motion. The recent approach in the development of a dynamic model for robotic mechanisms is to include the small motion deformations arising from the flexibility of the structure, hereafter referred to as small motion. These small motion deformations include bending, twisting, and axial extending.

Sunada and Dubowsky [Ref. 4] utilized the 4x4 transformation matrices including the effects of flexibility to describe the kinematics of flexible arm motion, specifically applied to industrial robots. The small motion deformations were superimposed on an assumed nominal large motion to include the effects of flexibility. This model ignored, however, the effect of the small motion interaction on the large motion, and consequently did not give a complete description of the actual motion dynamics. Sunada and Dubowsky utilized finite element method techniques and a method to discretize the distributed motion known as Component Mode Synthesis to obtain linear, ordinary, differential equations of motion.

Book [Refs. 5, 6] similarly included the small motion deformations in the 4x4 transformation matrices but he utilized a modal approach to model the flexible kinematics and truncated the series of assumed vibration modes. After application of Lagrange's equation and utilizing a combined set of large and small motion hybrid coordinates, a complicated set of dynamic equations of motion were obtained. The resulting equations of motion were non-linear in both large and small motion variables and were consequently time-consuming and expensive to solve.

Cannon and Schmitz [Ref. 7] utilized a similar modal approach with a Lagrangian formulation to model a single-link flexible arm. This particular model was obviously very restrictive in its application to robotic mechanisms. Cannon

and Hollars [Ref. 8] are investigating the modeling and control of two-link manipulators with flexible tendons, but it appears that the resultant dynamic model is likewise restrictive to this special application.

Truckenbrodt [Ref. 9] modeled the flexible manipulator as a "hybrid multibody system" consisting of both rigid and flexible elements. The application of his model was to a specialized example and compatibility between links was not clearly shown.

Huston [Ref. 10] developed the dynamic equations of motion for a flexible, multi-link manipulator utilizing a combination Newton-Euler approach and d'Alembert's principle. His assumption of a nominal large motion on which to apply the small motion deformations was similar to Dubowsky's and results in an incomplete representation of the actual motion dynamics.

Chang [Ref. 2] introduced an Equivalent Rigid Link System (ERLS) to describe the large motion kinematics. The small motion deformations were described relative to the Equivalent Rigid Link System. Applying finite element techniques and Lagrangian dynamics, two sets of coupled, non-linear, ordinary differential equations of motion were obtained. Because of the use of the ERLS, these sets of equations were composed of one set for large motions and one set for small motions. The set of large motion equations were non-linear in both the large and small motion variables.

The set of small motion equations were linear in the small motion variable and non-linear in the large motion variable. These particular characteristics of the resultant sets of equations of motion allowed for their relatively easy solution by a technique developed by Chang known as the Sequential Integration Method. Chang's model offered a complete representation of the dynamics of flexible manipulators as well as one that could be efficiently solved using the Sequential Integration Method.

The purpose of this research is to experimentally validate the accuracy of a dynamic model including flexibility. The dynamic model chosen is that developed by Chang. This model is tailored to a single-link flexible arm that was designed, constructed, and operated for the purpose of the dynamic model validation. Hydraulic actuation of the single-link arm is utilized and the motion of the arm is limited to a vertical plane. Computer simulation of the experimental flexible arm using the adapted dynamic model is on the IBM 3033. The integration methods from the Continuous System Modeling Program (CSMP) are utilized in the solutions of the dynamic equations of motion. Techniques for the acquisition of position data of the moving experimental arm are reviewed in a subsequent chapter. Photography and strain gauge measurement prove to be the most economical and simple procedures in this application.

The remainder of this thesis includes a chapter on the theoretical approach to model the dynamics of the flexible manipulator using the Equivalent Rigid Link System (ELRS). The Theoretical Approach chapter also includes a discussion on the modelling of the hydraulic actuation dynamics and a discussion of the computer simulation of the entire flexible manipulator system.

A chapter is devoted to a description of the experimental approach utilized in validating the dynamic simulation results. The chapter reviews the design of the experimental manipulator system, including the hydraulic actuation and the flexible arm. The Experimental Approach chapter also reviews various techniques investigated for experimentally determining the end-point position of the flexible manipulator.

The Results chapter follows and presents a comparison of the arm-tip position data obtained during the experimentation to the arm-tip position data obtained from the computer simulation. Also, a comparison is made between the actual strain of the experimental arm and the strain predicted by the ERLS dynamic model.

A chapter devoted to the control of flexible manipulators is included to provide a brief literature review on this aspect of flexible manipulator research. Additionally, an initial attempt at controlling the single-link flexible manipulator using the ERLS model is discussed.

Finally, a chapter each is devoted to drawing conclusions on the lessons learned in this research effort and for making recommendations on the future direction of research in flexible manipulators.

II. THEORETICAL APPROACH

Chang's dynamic model is based on his introduction of an Equivalent Rigid Link System (ERLS) to describe the large rigid motion of the flexible manipulator system. The small motion deformations are described relative to the ERLS. The local coordinate system for each link is defined in the ERLS and deformations are measured relative to this coordinate system. Coordinate transformation utilizing joint variables of the ERLS is applied to the actual deformed position at any point on a link to obtain the absolute position of that point. Time derivatives of the absolute positions are necessary for the kinetic energy derivation for use in Lagrange's equations.

It is necessary to discretize the deformations since these displacements are for each point along the flexible arm. The Finite Element Method (FEM) is utilized to accomplish this discretization of the deformations. The FEM nodal displacements represent the small motion deformations at the end of the link. A cubic shape function is assumed for each beam element. Choice of a cubic shape function ensures the complete representation of the displacement including rigid body rotation, translation, and compatibility of the displacement between elements.

After having described the kinematical relationships between the large and small motions, kinetics is introduced

to complete the derivation of the dynamic equations of motion. Utilizing the Lagrangian formulation requires the definition of generalized coordinates. The description of large and small motions are a logical choice for the generalized coordinates. The joint variables of the ERLS and the nodal displacements are the two sets of generalized coordinates utilized in Lagrange's equations. The kinetic energy has contributions from each link, actuators, and any loading. The potential energy has contributions from the elastic strain energy and from gravity. Generalized forces are included due to any applied forces and damping forces. After considerable effort in mathematical manipulations, rearrangements, and simplifications, the Lagrange equations yield two sets of non-linear, coupled, second-order, ordinary differential equations. One set of equations describes the large motions and the other set of equations describes the small motions, though both sets remain coupled. Details of the adaptation of Chang's ERLS model to the experimental, single-link, flexible arm are contained in Appendix A.

The equations of motion for the single-link flexible arm are written as two sets of equations, one set consisting of one equation for the large motion and one set consisting of two equations for the small motion as follows,

$$M_{QQ} \ddot{\theta} + M_{QN} \ddot{U} = F_Q \quad (1)$$

$$M_{NQ} \ddot{\theta} + M_{NN} \ddot{U} + K_N U = F_N \quad (2)$$

where,

MQQ is the 1x1 inertia matrix for large motions,
 MQN is the 1x2 coupled inertia matrix of the small motion
 contribution to the large motion,
 MNQ is the 2x1 coupled inertia matrix of the large motion
 contribution to the small motion,
 MNN is the 2x2 inertia matrix for small motion,
 KN is the 2x2 stiffness matrix,
 FQ is the 1x1 load vector for the large motion,
 FN is the 2x1 load vector for the small motion,
 θ is the generalized coordinate of the single joint
 variable representing the large motion,
 U is the 2x1 generalized coordinate vector of the
 deformations representing the small motion.

Utilizing hydraulic actuation for the single-link
 manipulator necessitates the derivation and the inclusion
 of the hydraulic actuator dynamics into the equations of
 motion of the flexible arm. The inclusion of the hydraulic
 power system dynamic equations into the flexible manipulator
 equations of motion involves the transformation of an input
 current to an output torque. The servovalve and actuator
 dynamics are included to make the description complete. Moog
 simplifies their servovalve dynamics to a single non-linear
 equation [Ref. 11],

$$Q = I K \sqrt{P_v} \quad (3)$$

where Q is the flow delivered from the servo valve,
 I is the input current,

K is the valve sizing constant computed from the flow conditions and is the servovalve contribution to the overall hydraulic system damping

P_v is the valve pressure drop and is equal to the difference between the supply pressure, P_s , and the load pressure drop, P_l .

The actuator dynamic includes the following continuity equation and the torque output equation [Ref. 12, pp. 133-138]

$$Q = D_m \dot{\theta} + C_{tm} P_l + \frac{V_t}{4 \beta_e} \dot{P}_l \quad (4)$$

$$T_d = \eta_t P_l D_m \quad (5)$$

where Q is flow delivered from the servovalve to the actuator,

$D_m \dot{\theta}$ is the flow component causing actuator rotation,

$C_{tm} P_l$ is the leakage flow in the actuator,

$\frac{V_t}{4 \beta_e} \dot{P}_l$ is the compressibility flow,

T_d is the required torque delivered to move the load and to overcome inertia,

η_t is the torque efficiency,

D_m is the motor displacement,

$\dot{\theta}$ is the actuator motor angular velocity,

\dot{P}_l is the time derivative of the load pressure drop, P_l ,

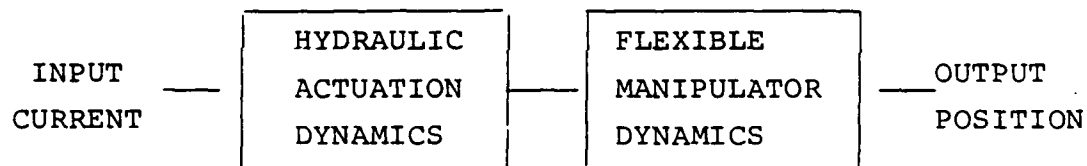
C_{tm} is the total leakage coefficient of the actuator and is the actuator contribution to the overall hydraulic system damping

V_t is the total compressed volume including actuator lines and chambers,

β_e is the effective bulk modulus of fluid.

Values for each of these parameters are computed from the actuator specifications and from good engineering judgement.

The following diagram shows the transformation of the input current to an output position and includes the hydraulic and flexible manipulator dynamics,



The preceding hydraulic dynamic equations and relationships are incorporated into the main computer program for solving the dynamic equations of motion for the experimental single-link flexible arm listed in Appendix B.

Computer simulation of the equations of motion for the experimental arm and hydraulic actuator required the solution of three simultaneous, non-linear, coupled, second-order, ordinary, differential equations. Fortran language and the double precision, variable-step, fourth-order, Runge-Kutta

integration method available through the Continuous System Modeling Program (CSMP) are utilized in coding the simulation.

Eq. 1 and 2 can be substituted into a matrix format to create a 3x3 coefficient inertia matrix and a 3x1 right-hand side of forces and moments. The unknowns become the large motion joint variable acceleration and the small motion deformation vector accelerations. The matrix format appears as follows:

$$\begin{bmatrix} MQQ & MQN \\ MNQ & MNN \end{bmatrix} \begin{bmatrix} \ddot{\theta} \\ \ddot{U} \end{bmatrix} = \begin{bmatrix} FQ \\ FN - KN U \end{bmatrix}$$

Construction of the computer coding involves forming each of the elements of the coefficient inertia matrix and the force/moment vector in a separate subroutine. Once formed the elements are assembled into the matrix after which an IMSL linear equation solver subroutine is used to solve for the accelerations. The accelerations are integrated twice using the double precision, variable-step, fourth-order, Runge-Kutta integration method available through the Continuous System Modeling Program (CSMP). Finally a transformation from local coordinates to global coordinates takes place to get global position information on the motion of the arm tip.

Initially, the single-link parameters and the motion variables initial conditions are input. There is also a need to form the various transformation, inertia, and assorted other matrices for use later in the inertia and force/moment matrix subroutines. Another prerequisite for constructing the equations of motion are subroutines for doing matrix multiplication and addition, and for doing the matrix operations of the transpose and the trace. These subroutines are all listed in the copy of the coding in Appendix B.

Results from the computer simulation and their comparison to the actual experimental motion data are discussed in the Results chapter.

III. EXPERIMENTAL APPROACH

The experimental validation of the Equivalent Rigid Link System (ERLS) dynamic model on a single-link flexible manipulator required a significant preliminary design effort. The power system for the experimental arm needed to be chosen, designed, and purchased. Detailed design of the single-link flexible arm needed to be completed and the arm needed to be manufactured. Techniques for the measurement of the position versus time of the flexible arm tip needed to be investigated and a suitable technique chosen. The power system and the experimental single-link flexible arm finally needed to be assembled into an operational system and the arm tip position measurement technique needed to be implemented.

It was decided to choose a hydraulic system to power the experimental arm. The reasons for this choice included the desire to increase the Mechanical Engineering Departments' exposure to hydraulics and to utilize the knowledge gained while taking the Fluid Power Control course. The Naval Surface Weapons Center, White Oak, located at Silver Spring, Maryland agreed to fund the purchase of the required components of the hydraulic power system as a result of their support of the robotic research effort in the Mechanical Engineering Department at the Naval Postgraduate School.

The design of the hydraulic power system involved the selection of the appropriately sized actuator, servovalve, and power unit, as well as the selection of a suitable servo-controller, high pressure filter and position transducer. Miscellaneous hoses and fittings were obviously also required for the final system assembly.

The power supply selected was a York hydraulic power unit that was available in the Mechanical Engineering Department. This unit was overhauled and upgraded to include a 3 horsepower motor and starter to increase the system supply pressure to 2250 psi.

The selection of the servovalve and actuator required the following analysis [Ref. 12: pp. 81, 133-138]

1. Assume a load description of the form

$$J \ddot{\theta} + T_1 = T_d$$

where J is the total moment of inertia of the arm and the load reflected from the base,

T_1 is the maximum load torque including the weight of the arm and maximum loading (15 lbf) in the horizontal position,

T_d is the required torque delivered to move the load and to overcome inertia,

$\ddot{\theta}$ is the actuator motor angular acceleration

2. Assume a design point of $\dot{\theta}=45$ deg/sec, $\ddot{\theta}=45$ deg/sec²

3. The given geometry and dimensions of the arm and loading results in the following total inertia,

$$J = 74.6942 \text{ in-lbf-sec}^2.$$

4. The maximum load torque including the weight of the arm and the loading is,

$$T_1 = 804.380 \text{ in-lbf.}$$

5. Assume the system supply pressure, P_s , is 2000 psi and that the load pressure drop, P_1 , is $2/3$ of $P_s = 1333.3$ psi. Assume the torque efficiency is worst case, $\eta_t = .6$.

The required displacement of the motor, D_m , is therefore,

$$D_m = \frac{T_d}{\eta_t P_1} = 1.0788 \text{ in}^3/\text{rad}$$

The selected actuator must at least have this displacement. Bird-Johnson's 3-axis Hyd-Ro-Wrist with a displacement in the pitch axis of $4.0 \text{ in}^3/\text{rad}$ was chosen. The wrist additionally has yaw and roll axes each with a $1.0 \text{ in}^3/\text{rad}$ displacement. However, in this thesis research only the pitch axis was utilized and the yaw and roll axes were removed.

6. The selection of the servovalve required an estimation of the flow delivered to the actuator at design conditions. The continuity equation (Eq. 4) describes the flow to the actuator.

At design conditions \dot{P}_1 is assumed zero. After using good engineering judgement in assuming values for each parameter, the design flow corrected to rated conditions becomes,

$$Q\text{-design} = .637 \text{ gpm}$$

Moog 760-100 servovalve having a 1.0 gpm rated flow was selected.

7. A Moog servocontroller and a high pressure filter assembly were chosen to complete the hydraulic power system. A Bourn potentiometer will be used to extract large motion rotation data for use with the photography measurements in determining arm tip position.

Ideas for the design of the experimental arm were initially investigated by visiting the robotic research laboratories at Stanford University and at SRI International. The experimental flexible manipulator systems utilized by Cannon at Stanford and by Andeen at SRI provided valuable information for the design of the experimental arm [Ref. 7]. Figures 1, 2 and 3 are photographs of the experimental flexible arm and the hydraulic power system. The basic configuration of the arm includes two parallel, flexible, steel, flat bars connected by thin steel strips to transverse steel bridges. The parallel flat bars provide for flexibility in a vertical plane only. This flexibility is minimally hindered by the transverse bridges because of the thin, connecting, flexible

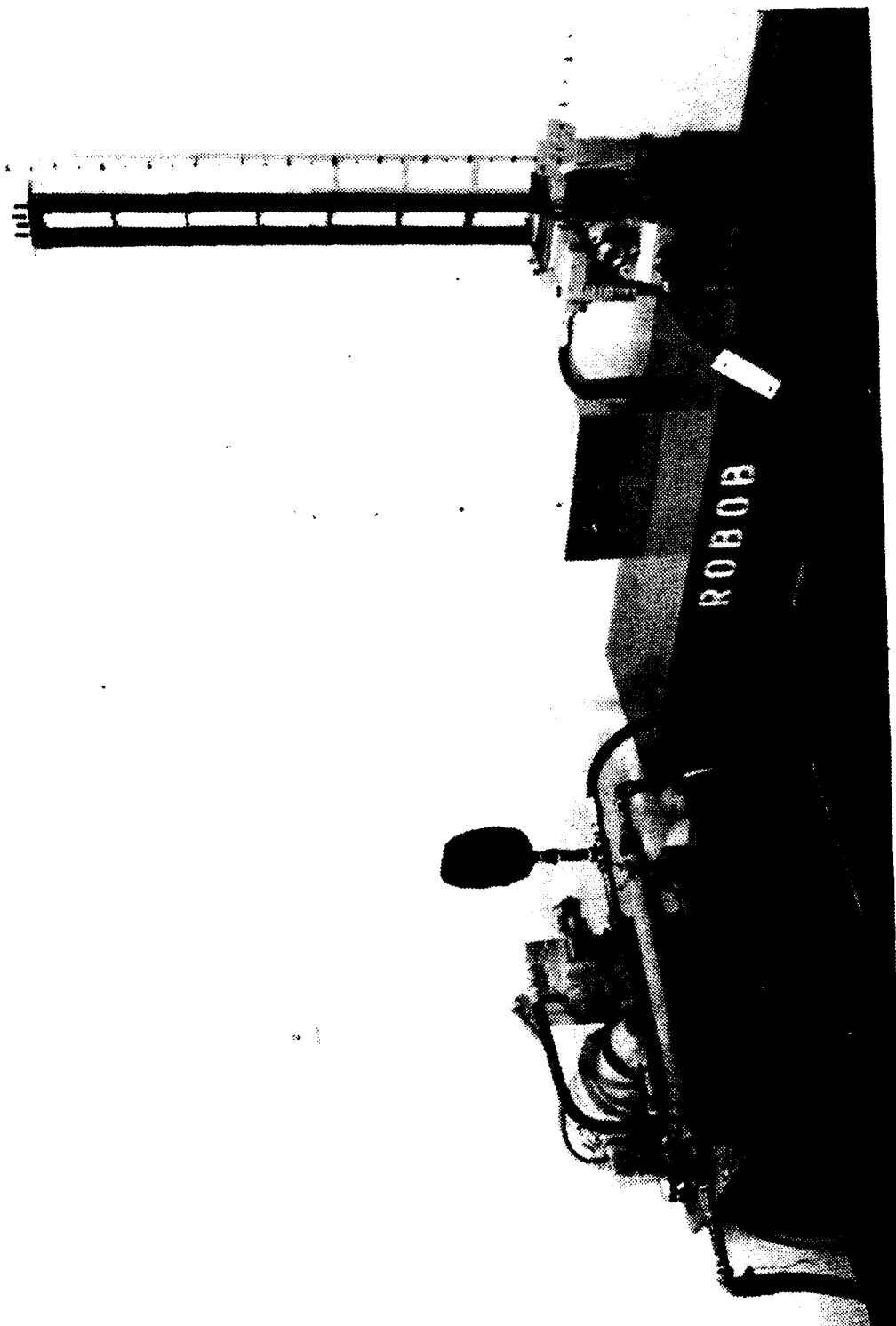


Figure 1. Single-Link Flexible Manipulator System.

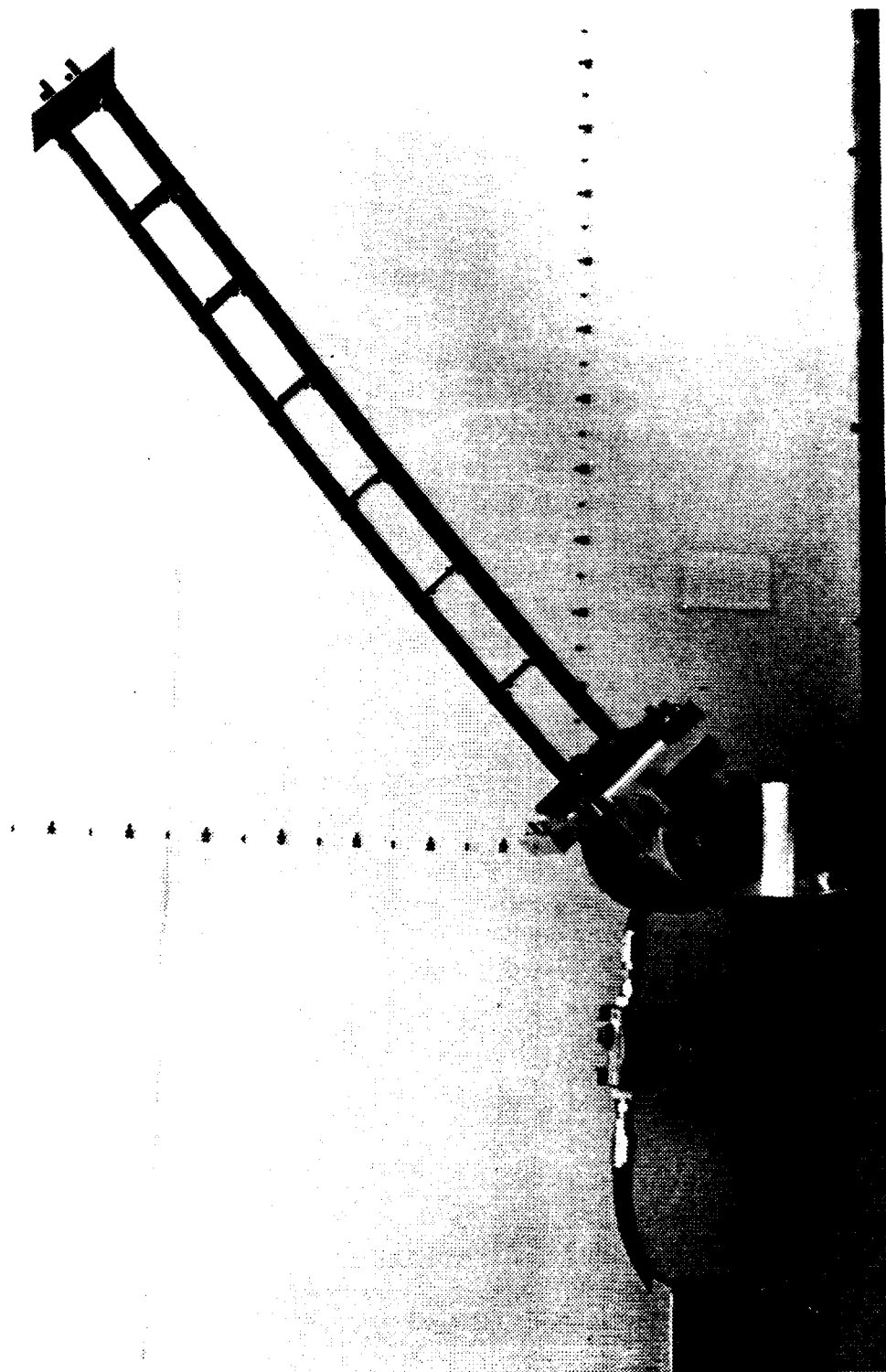


Figure 2. Manipulator in an Intermediate Vertical Position.

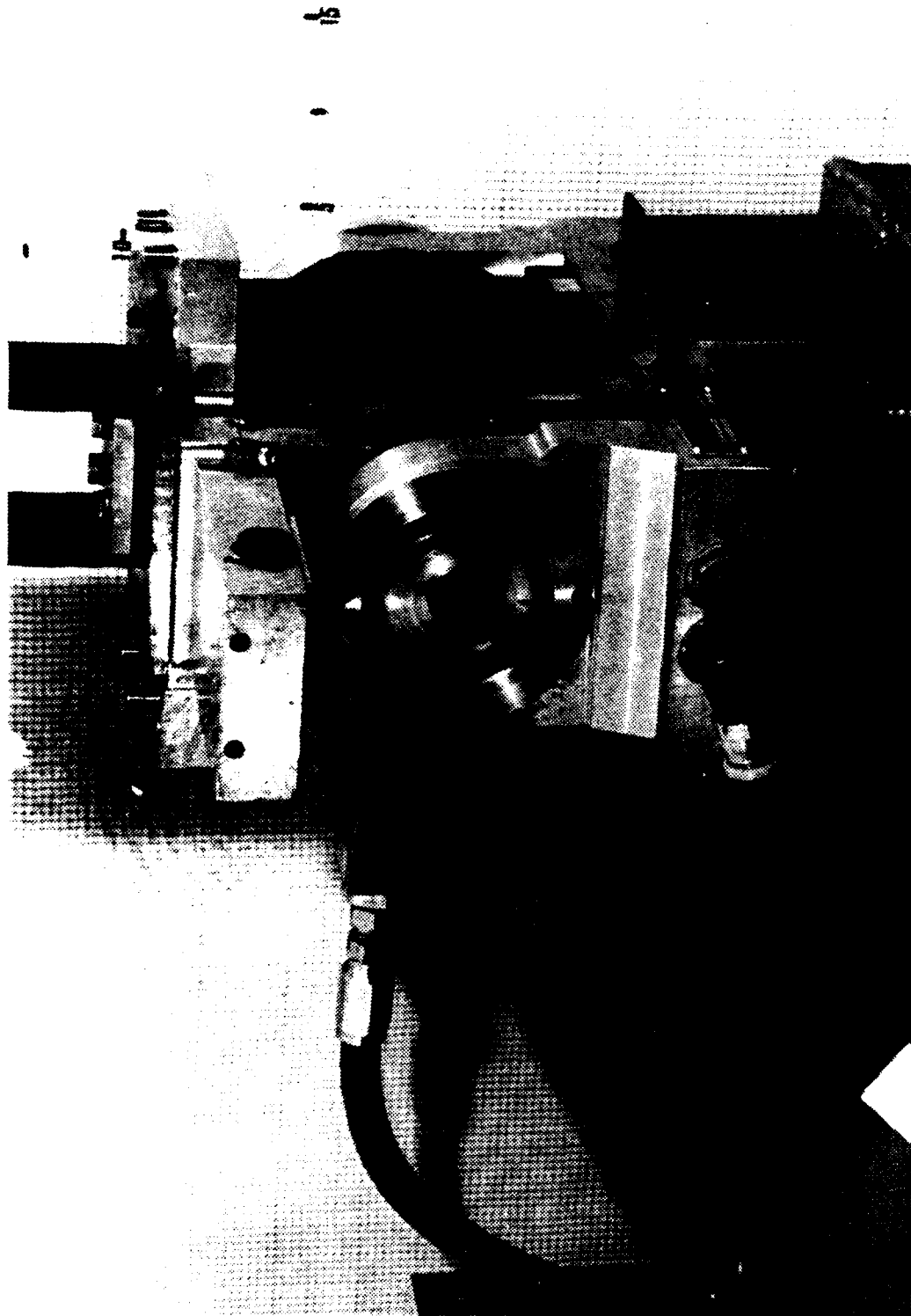


Figure 3. Hydraulic Rotary Actuator.

strips. The transverse bridges increase torsional rigidity and reduce the tendency of the arm to twist while in motion. Figure 4 is a photograph showing the inclusion of the transverse bridges in the flexible arm construction. External loading is attached to the arm tip end transverse bridge by the securing of the load on the four welded studs. The hydraulic actuator is attached to the other end of the flexible arm.

The validation of the ERLS dynamic model requires the comparison between the predicted arm tip position from the model and the actual arm tip position from the experimental single-link manipulator. The computer program listed in Appendix B generates the flexible arm tip position referenced to a planar, global coordinate system having the origin at the hydraulic actuator rotation axis. The problem of determining the arm tip position of an experimental, flexible manipulator is far more difficult than that experienced in determining the arm tip position of a rigid manipulator. There is currently a significant research effort in developing accurate techniques for arm tip position measurement and control of a flexible manipulator. A brief summary of the techniques investigated for possible use in this thesis research follows.

The first technique considered was the crude but effective method of taking motion pictures of the arm against a grid background with a time counter in the field of view.

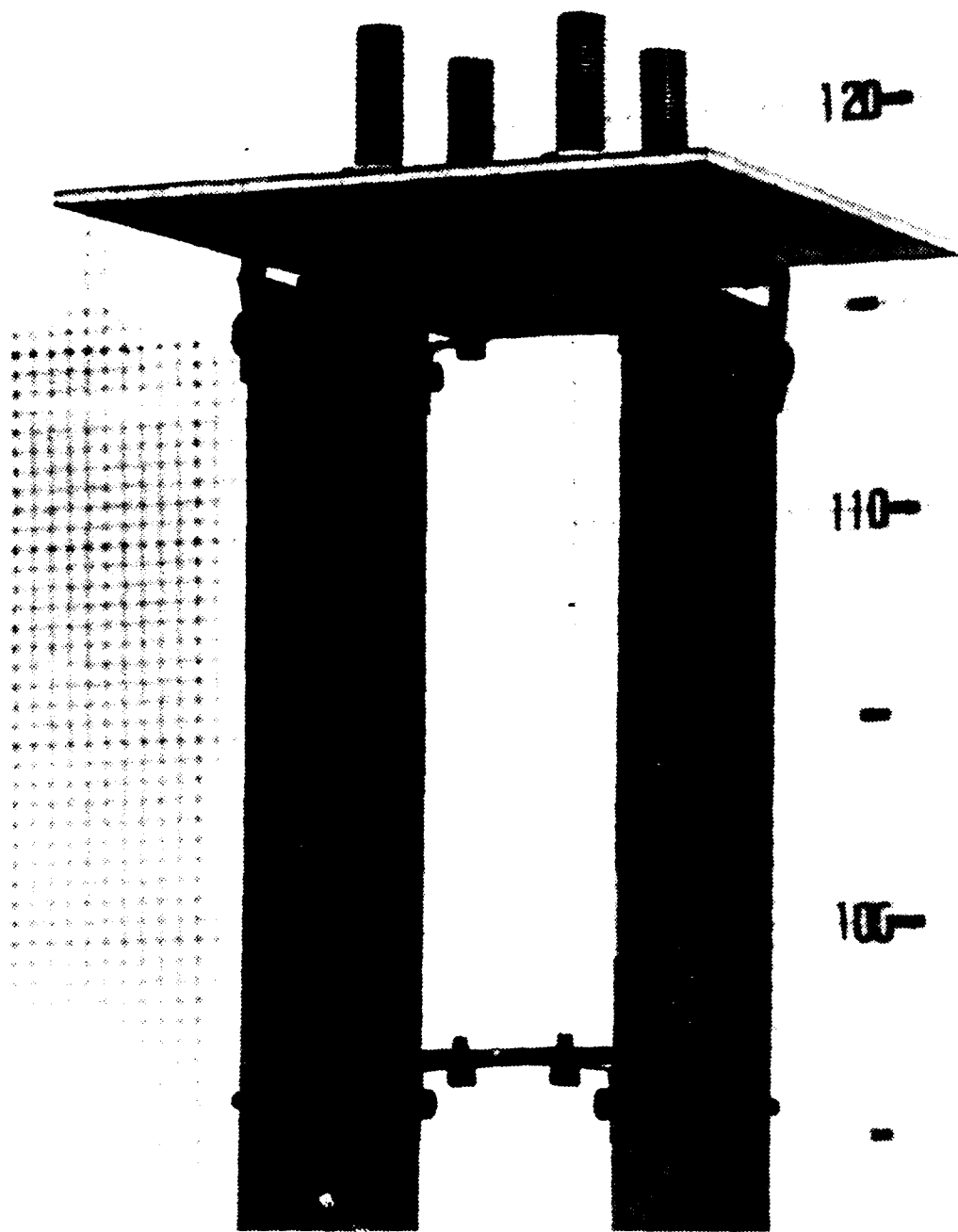


Figure 4. Flexible Manipulator Showing Transverse Bridges, Tip Loading and Grid Background.

The arm tip position at any time is manually determined on each picture frame by counting the number of grid lines in the vertical and horizontal directions.

Cannon and Schmitz [Ref. 7] utilized an optical sensing system of a focusing lens, a photodetector, an amplifier, and an A/D converter to acquire position data from their horizontally moving, flexible arm. An incandescent light bulb was affixed to the tip of the arm and provided the light intensity that was received by the optical sensing system. This technique appeared to be suitable for its specialized application, but may not be as satisfactory in general usage.

The National Bureau of Standards has conducted manipulator end-point position sensing experiments using an automatic laser tracking interferometer system. Initial experiments have provided very promising results [Ref. 13]. The significant drawbacks to this laser tracking technique were its current high cost and complicated technology.

Andeen has utilized strain gages and extrapolated the deflection to the arm tip assuming first mode vibration. This technique was relatively simple, but may be inaccurate unless the predominant mode of vibration is the first mode.

Interfacing the planar motion of the flexible arm to a digitizing tablet provided a potentially feasible technique for acquiring arm tip position. This technique would allow for automatic, time-efficient, position data acquisition.

This technique was obviously only applicable to planar motion of the manipulator and was expensive to implement for large motion excursions of the arm.

Lt. William M. Dunkin [Ref. 14] conducted research at the Naval Postgraduate School on the use of ultrasonics for a position reference system of a manipulator arm. His work was preliminary in nature and his experiments utilized a stationary manipulator. Despite the poor accuracy of the results, use of ultrasonics for arm tip positioning and control has significant potential if further research continues to perfect this technique.

Use of a position/displacement transducer that provided an electrical signal proportional to the linear extension of a cable offered another technique for automatic, position data acquisition. Arranging a transducer on each planar coordinate axis and affixing each cable to the arm tip would allow for accurate positioning to occur. To utilize this measuring technique would require the inclusion of the cable tension in the arm dynamic equations of motion.

Use of accelerometers followed by two electrical integrations to yield position information offers good frequency response and are commercially available. Use of a digitizing vision system for automatic position data acquisition has great promise for future robotic applications, but is currently very expensive to implement. [Ref. 15]

For this research the use of motion pictures and strain gages were selected based on the availability, simplicity, and cost. The use of motion pictures in planar applications, though tedious, can provide excellent results of arm tip position data. Strain gages are utilized to compare the actual strain of the experimental arm to the strain predicted by the ERLS dynamic model.

IV. RESULTS

The validation of the ERLS dynamic model includes a comparison between the actual arm tip position and the predicted arm tip position. The actual arm tip position measurements were obtained by taking motion pictures of the experimental arm and by a frame-by-frame examination of the motion. As an additional check, the utilization of strain gages allowed for a comparison between the actual strain of the experimental arm and the strain predicted by the ERLS dynamic model.

Evaluation of the plots of experimental and theoretical position or strain requires a comparison criteria. Frequency and amplitude are the parameters utilized in establishing the criteria for comparison. Similarity in frequency content and amplitude is necessary for determination of proper control action in the closed-loop servo system design and for an accurate representation of the actual motion in any flexible manipulator machinery design application. A relative percentage error of $\pm 10\%$ from the experimental results is considered the standard for comparison. The strain amplitude and frequency errors are computed by taking the difference between the theoretical and experimental strain values. The strain amplitude is a combination of both fundamental and second mode amplitudes but examination of the plots reveals

that the first mode amplitude is dominant. The strain frequency error is separated into the fundamental and second mode errors. The tip position amplitude error is computed by taking the square root of the sum of the squares of the differences between the theoretical and experimental X and Y coordinate positions. The tip position frequency errors are computed by taking the difference between the theoretical and experimental tip position frequencies. Only the first mode frequency and amplitude errors are determined for the arm tip position. The normalization of the absolute error to a relative error is accomplished using the arm length for the tip position amplitude measurements and the experimental strain amplitude for the strain amplitude measurements. The experimental frequencies are used for normalizing the tip position and strain frequency errors. This normalization is accomplished in order to compute the appropriate order of magnitude error between the theoretical predictions and the experimental results.

Figures 6, 7, and 8 are plots for three loading conditions of the comparison of experimental to theoretical arm tip positions in the global X (horizontal) and Y (vertical) coordinate directions. The three loading conditions are the no-load condition, the 5 pound load condition, and the 10 pound load condition. The excitation of the hydraulic actuation for all three loading conditions is a step input of 4 milliamps current. The initial condition for these experimental runs is the horizontal position of the flexible

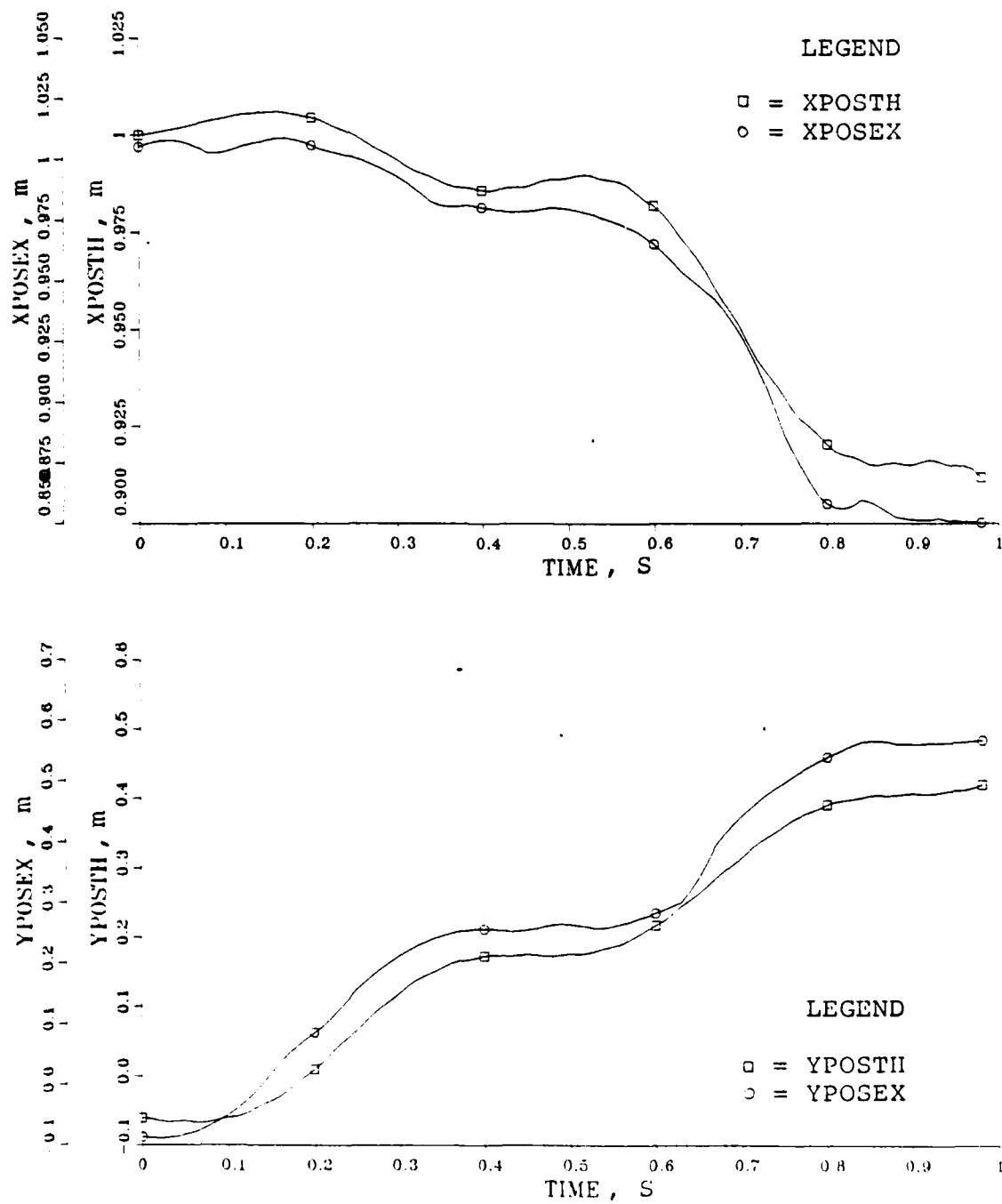


Figure 6. X and Y Tip Position For No Load.

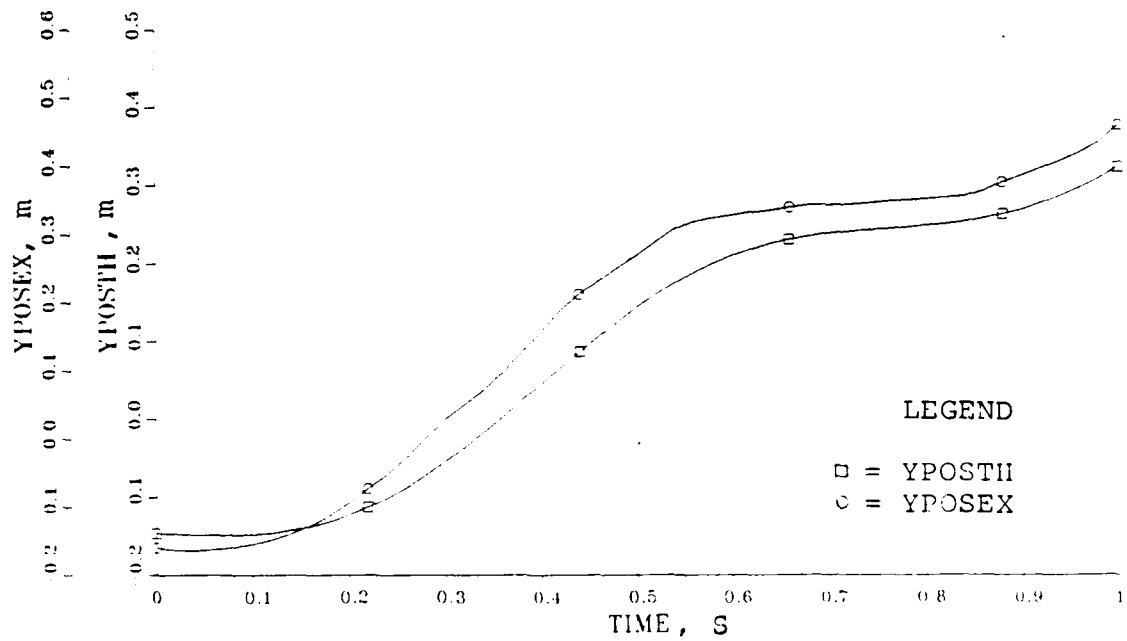
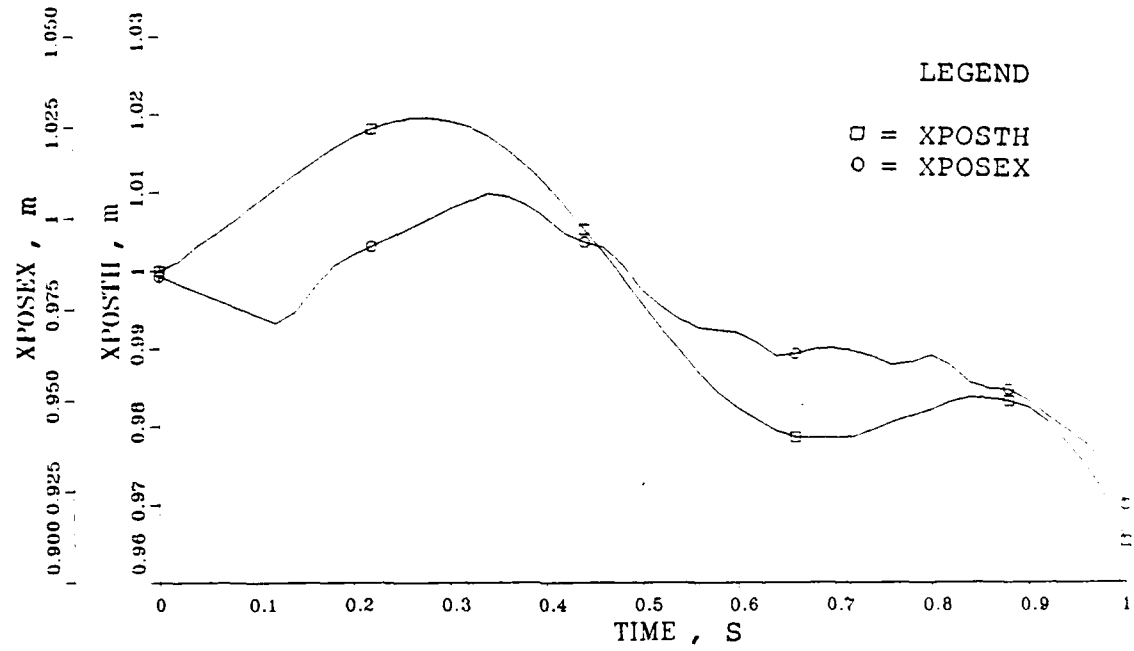


Figure 7. X and Y Tip Position For 2.115 Kg Load.

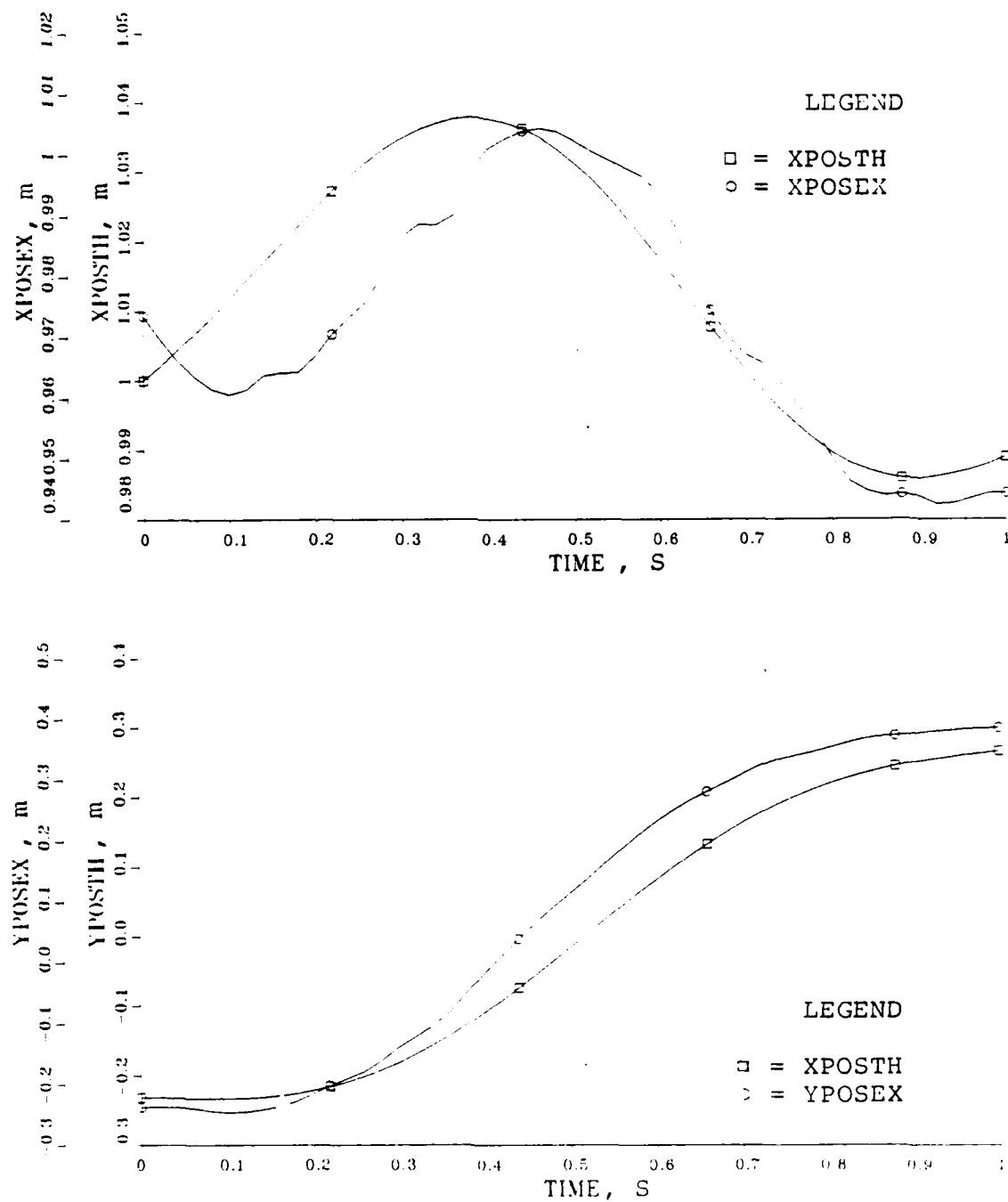


Figure 8. X and Y Tip Position for 4.23 Kg Load.

arm. Experimental arm tip position data requires a preliminary parallax correction and a geometric transformation prior to plotting. The parallax correction is necessary because of the relatively close proximity of the camera to the experimental arm motion. The geometric transformation is necessary because of the offset of the base of the experimental arm from the axis of rotation of the hydraulic actuator.

Four CEA-06-12UW-350 strain gages are installed on the flexible arm. Two are placed on opposite sides of the neutral axis at the base and at the mid-longitudinal position of the arm. Consequently, two gages provide tensile strain readings and two gages provide compressive strain readings. A mid-longitudinal position gage is selected for plotting strain data because of the higher sensitivity, and consequently better resolution, in the strip chart recording. The theoretical strain predicted by the ERLS dynamic model in the mid-longitudinal position is computed from the Finite Element shape matrix describing the transverse or bending displacement of the flexible arm. The derivation of the theoretical strain is included in Appendix C. Figures 9, 10 and 11 are plots for the three loading conditions of the comparison of experimental to theoretical microstrain. Excitation of the hydraulic actuation for all three loading conditions is a step input of 4 milliamps current. The initial condition for these experimental runs is the vertical position of the flexible arm.

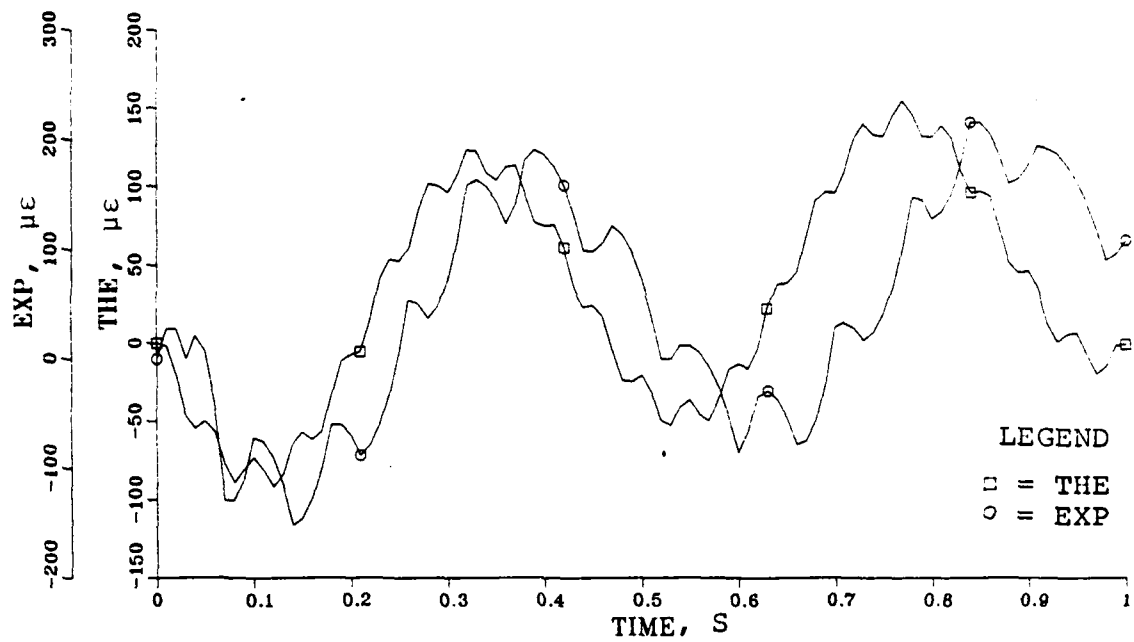


Figure 9. Microstrain For No Load.

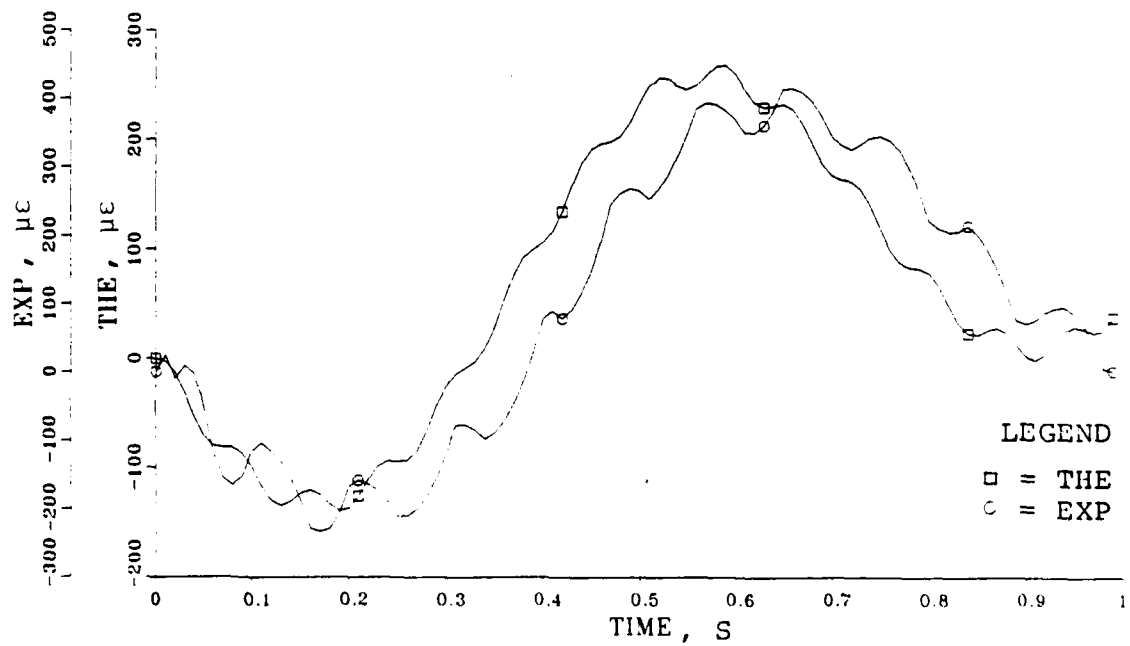


Figure 10. Microstrain for 2.115 Kg Load.

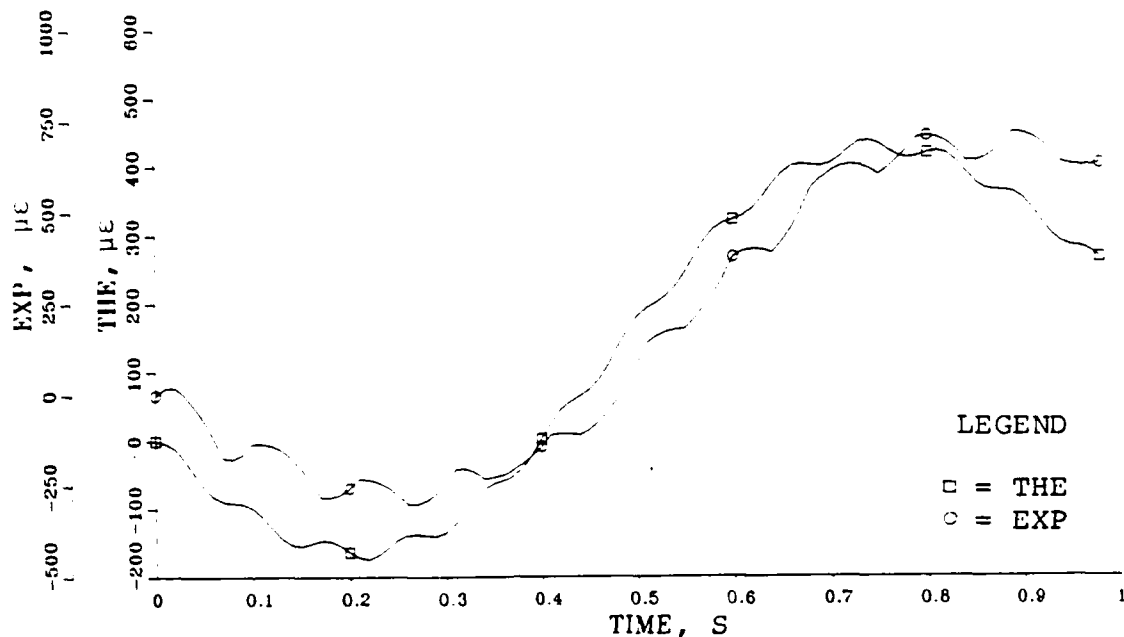


Figure 11. Microstrain For 4.23 Kg Load.

Utilization of the evaluation criteria of $\pm 10\%$ error reveals the tip position amplitude error is acceptable. This is significant considering the importance of tip position accuracy as a criteria for evaluating robot performance. Because of the lack of adequate tip position accuracy for certain applications a significant research effort is ongoing to develop appropriate tip sensors to compensate for the position errors. The acceptable tip position amplitude error despite the single element modelling allows for relatively accurate predictions of tip position motion and consequently suggests the potential usefulness of the ERLS model in improving the tip position accuracy. Table I lists

the relative percentage errors of tip position amplitude for the different loading conditions given a 4.0 milliamp input current to the servovalve.

TABLE I
RELATIVE PERCENTAGE ERRORS OF TIP POSITION AMPLITUDE

No Load	10.7
2.11 Kg Load	10.5
4.23 Kg Load	11.5

The differences in amplitude observed in the arm tip position measurements are attributed to the error in recording the experimental position data, to the single element modelling of the experimental arm, and to the small displacement assumption of the vibration. Specifically, the frame-by-frame examination of the arm tip position is hindered by the lack of clarity of the arm tip and by the absence of definition of the background grid measurement lines. Improvement in the grid spacing and color intensity and in the camera exposure setting would improve the quality of the recorded data. The increased rigidity resulting from the single element model of the experimental arm is responsible for the amplitude of the theoretical X tip and Y tip

position data to be less than the experimental position data and would increase as the number of elements is increased in the model.

Axial deformations are neglected and small bending displacements are assumed in the theoretical modelling of the experimental arm. The effect of these assumptions is noticed in the comparison of the X coordinate arm-tip position during the first few tenths of a second of motion. The experimental arm tip position actually decreases during this initial time period. The theoretical model predicts an increase in arm tip position, particularly during the heavier loading conditions. Figure 12 illustrates how the theoretical model could predict an increase in the X coordinate tip position. The theoretical arm position approximates the actual arm position and because the small motion displacement is measured with respect to the ERLS local coordinate axis the theoretical arm length appears to increase. This arm length increase is especially amplified with large displacements which result from heavier loading. For smaller displacements the arm length increase is negligible. The increase in the arm length is reflected by an increase in the theoretical X coordinate tip position.

The motion pictures were taken at a camera speed of 24 frames per second. Since the fundamental and second mode frequencies of the experimental arm without any load are 2 hertz and 13 hertz respectively, only the fundamental

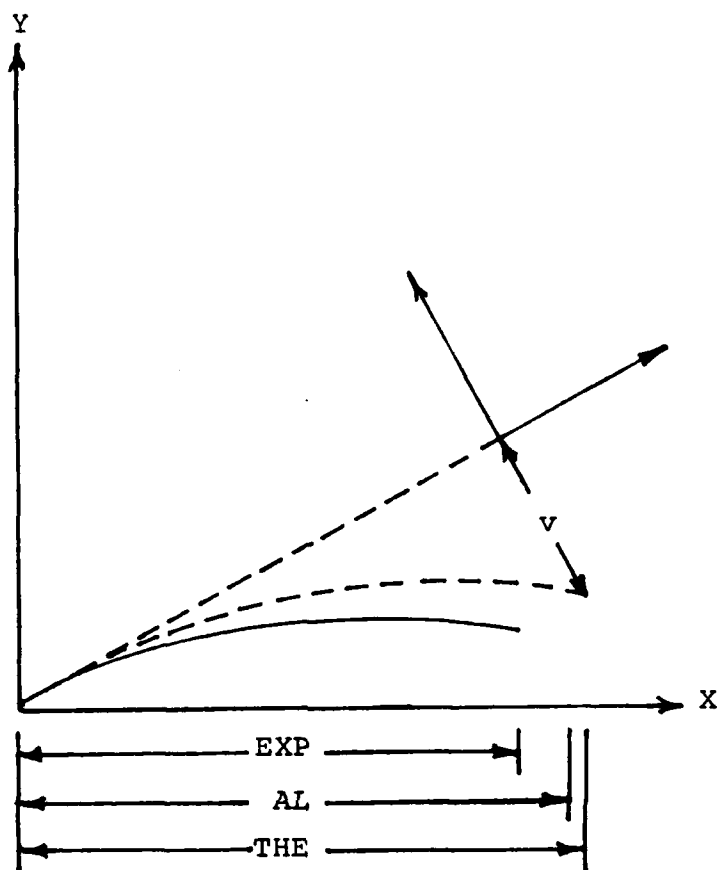


Figure 12

- - -	ERLS and Theoretical Arm Position
—	Experimental Arm Position
EXP	Experimental X-Coordinate
AL	Actual Experimental Arm Length
THE	Theoretical X-Coordinate
v	Theoretical Arm Tip Displacement

frequency is observed by the motion pictures. Comparison of the frequency content of the experimental and theoretical arm tip position reveals close agreement for the fundamental frequency. Comparison of the frequency content of the experimental and theoretical strain reveals that the experimental results have lower frequency content compared to the theoretical results in both the fundamental and second mode frequencies. Utilization of the evaluation criteria reveals the standard of $\pm 10\%$ relative percentage error is exceeded for the second mode frequency using the strain measurements. Table II lists the relative percentage errors of the frequencies for the different loading conditions given a 4.0 milliamp input current to the servovalve.

TABLE II
RELATIVE PERCENTAGE ERROR OF FREQUENCIES

Strain Data	Fundamental	Second Mode
No Load	5	38
2.115 Kg Load	5	26
4.23 Kg Load	6	22

Tip Position Data	Fundamental
No Load	5
2.115 Kg Load	5
4.3 Kg Load	5

The no-load theoretical fundamental and second mode frequencies are predicted to be 2 hertz and 18 hertz respectively. The difference in frequency content between the theoretical predictions and the experimental results is explained in that only one element from the Finite Element Method is utilized in modelling the experimental arm. The single element model limits the number of degrees of freedom, and consequently the flexibility, of the dynamic model. The dynamic model therefore appears more rigid than the actual experimental arm. Increasing the number of elements in modelling the experimental arm would increase the flexibility of the dynamic model which would reduce the frequencies of predicted motion. Error between the experimental and theoretical results is additionally introduced by the limited resolution of the strain measurements from the strip chart recorder.

Utilization of the evaluation criteria reveals the standard of $\pm 10\%$ error is exceeded for strain amplitude measurements. Table III lists the relative percentage errors of strain amplitude for the different loading conditions given a 4.0 milliamp input current to the servovalve. The amplitude of the theoretical strain measurements are typically less than the experimental strain measurements in both the fundamental and second mode frequencies. This observation is again explained by the limitation on flexibility imposed by the single element model of the experimental arm. Increasing the number of elements in modelling the experimental arm would

increase the flexibility of the dynamic model which would result in increased amplitudes of predicted strain.

TABLE III
RELATIVE PERCENTAGE ERRORS OF STRAIN AMPLITUDE

Strain Data	
No Load	38
2.115 Kg Load	38
4.23 Kg Load	41

Table II indicates that the relative percentage error of the first mode frequency increases slightly while the error of the second mode frequency decreases as the loading is applied. Tables I and III indicates that the relative percentage error of the tip position and strain amplitudes increases slightly as the loading is applied. As mentioned before, the first mode amplitude is dominant. With increased loading the experimental arm becomes softer or more flexible. The dominant first mode strain amplitude and the first mode tip position amplitude are slightly more difficult to predict as the arm flexibility increases. This observation is consistent with the slight increase in error in the first mode frequency as the loading increases. These trends are consistent with the previous observations that the theoretical predictions result in a stiffer system compared to the experimental results.

In other words, the single element model better predicts the first mode amplitude and frequency of a stiff system compared to a softer system. As the loading increases resulting in a more flexible system, the first mode strain frequency and dominant first mode strain amplitude errors increase slightly. Similarly, the first mode tip position amplitude error increases slightly.

The trend of the strain second mode frequency error initially appears as an anomaly since the error decreases as the loading increases. This trend contradicts the expected result that is observed in the first mode frequency and amplitude error trends. The trend in the second mode frequency error suggests that the theoretical model more easily predicts the second mode frequency of a softer system. In other words, the theoretical model is better suited for predicting the second mode frequency in a flexible system. The accuracy of the theoretical model to predict the experimental arm deformation is dependent upon the shape function approximation of the natural modes. The choice of the shape function described in Appendix C to describe the deformations results in the observed trend in the strain second mode frequency error with loading.

Investigation of the predicted and actual strains for an excitation of 3.0 milliamps current to the servovalve was made and revealed similar trends in frequency and amplitude errors as noted in the 4.0 milliamps case. As expected, the

maximum strains achieved and predicted are less in the 3.0 milliamps case. However, the relative error percentages in the 3.0 milliamps case are not any less than the 4.0 milliamps case. This suggests that the small displacement assumption has little effect on increasing the strain amplitude and frequency errors as the strain is increased. However, this suggestion is obviously limited to this particular experiment and needs to be investigated for other values of excitation current.

The assumptions of single element modelling, of small displacement theory, and of no axial deformation are made for analytical expediency and for computational efficiency. The validity for making these assumptions should be reviewed in light of these experimental results.

The importance of correct modelling of the hydraulic dynamics was emphasized when the interaction of the hydraulic actuation, the gravitational force, and the arm movement from the vertical plane created a serious resonance problem. This phenomenon was observed during the theoretical strain simulations and resulted in serious instability after approximately one second of motion. Investigation revealed that the hydraulic damping was improperly modeled. The resonance was eliminated after a modification to the damping was made.

V. CONTROL OF FLEXIBLE MANIPULATORS

The advantages to employing flexible manipulators is well documented in the literature [Ref. 16: pp. 101, 102]. However, flexible manipulator usage in industry has been minimal principally as a result of the difficulty to control the flexible manipulator end-effector [Ref. 3: p. 1209]

There has been considerable research recently in the development of flexible manipulator control strategies using state-space model techniques. A brief survey of this research follows.

Cannon and Schmitz [Ref. 1] introduced the concept of end-point position feedback for use in controlling flexible manipulators. The end-effector position was sensed and was fed back to the controller for subsequent determination of the control action required by the joint actuators. Use of end-point position feedback would increase the response speed and would allow for the use of lightweight flexible manipulators. Techniques for determining the position of the manipulator end-point were reviewed in the Experimental Approach chapter.

Cannon and Schmitz [Ref. 7] utilized a modal approach with a Lagrangian formulation to model a single-link flexible arm. Both large motion rotation and small motion deformations of the flexible arm were included in a single variable in the

formulation. The state-space model resulted in a set of decoupled differential equations where the states included the rigid body mode and the flexible modes. Cannon and Schmitz limited the state-space model to include only the first three flexible modes. The flexible mode states included contributions from large motion rotation as well as small motion deformations. The joint actuator provided direct control action to the large motion rotation of the arm. Since the flexible mode states included coupling between the large and small motions, the joint actuator provided control action to the small motion deformations as well. This ensured state controllability of the state space model. Output controllability was ensured after determination of the arm-tip sensor and the joint-rate sensor measurement vectors in the state-space output equation. The joint angle and rate were measured with a potentiometer and a tachometer, respectively. Since all flexible mode states were not measurable, Cannon and Schmitz included an estimator in the feedback control system to ensure that the system was observable. The Linear Quadratic Gaussian (LQG) approach was utilized in the controller design. Experimental verification of the feedback control system on a single-link flexible manipulator demonstrated that stable and precise position control of the end-effector was achievable.

Book and Hastings [Ref. 5] similarly utilized a Linear Quadratic Regulator approach in designing a controller for a

flexible manipulator. Their state-space model consisted of a rigid body mode state and the first two flexible modes as subsequent states. Their initial formulation of the dynamic equations of motion included coupling between the rigid body mode and the flexible modes, and ensured state controllability. Output controllability was ensured after determination of the strain gauge sensor, joint-position sensor, and joint-rate sensor measurement vectors in the state-space output equation. The modal deflections were measured from strain gauge data. Observability was ensured by including an estimator in the feedback control system to estimate the two unmeasured modal velocities. Minimizing the first two open-loop modal resonances in an experimental single-link flexible manipulator confirmed the feedback control system's ability to control the flexible modes. One significant difference between the Book and Hastings model and the Cannon and Schmitz model was that the former utilized flexible modes corresponding to fixed-free beam vibrations whereas the latter utilized pinned-free beam vibrations. The fixed-free flexible mode model allows for a more accurate extension to the multi-link manipulator since fixed link boundary conditions describe the multi-link physical system.

Adaptation of Chang's Equivalent Rigid Link System flexible model [Ref. 2] to the single-link manipulator provided another alternative to the modal approach in defining state variables. Defining both large motion rotations and small motion deformations as generalized coordinates in the Lagrangian formulation

of the dynamic equations provided an easy extension for these coordinates to become state variables. A comparison of the state-space model to the ERLS non-linear model was needed to determine the range of the applicability of the linearized model away from the operating point. Comparison of simulations of open loop large motion rotation, theta, and small motion deformations indicated reasonable agreement between the state-space model and the ERLS non-linear model for approximately 1.5 sec. or 120 degrees after an input torque of 5 N-m was applied.

The state space representation provided the input to the NPS mainframe optimal feedback controls program CONTROLS, subprogram OPTSYS, to design an LQR optimal controller. Coupling between the large and small motions included in the Lagrangian dynamic equation formulation ensured state controllability. After assigning arbitrary identity matrices for the output measurement matrix and the weighting matrices for the quadratic performance index, an optimal feedback gain control matrix was computed by the OPTSYS program. Details of the linearization and state-space representation of the ERLS model and the optimal feedback control design are included in Appendix D. The definition of the output measurement matrix assumed the feedback loop was closed utilizing tip control. Simulation of the state-space model closed-loop response to an initial condition of a 20 degree rotation away from the zero degree operating point, a -.03

meter tip deflection and a $-.1$ tip slope confirmed the linear feedback control systems' ability to control the state-space model of the single-link flexible arm. A graph of the linear system closed-loop response of the large motion rotation, θ , is plotted in Figure 13. This result gives some confidence in the linear controller's ability to control the non-linear model given small perturbations about the operating point. However, simulation of the linear controller with the non-linear model is necessary to investigate the range of operation.

Utilizing the arm-tip deflection and slope as state variables appears to be an improvement over the flexible mode state variables since the former are more easily measurable quantities. The need for an estimator in the feedback control system may be eliminated. However, additional comparison and investigation of the merits of both approaches are necessary. From the results obtained from other research it appears that control of a single-link flexible manipulator is realizable. Extension of these feedback control system approaches to multi-link flexible manipulators is necessary if the advantages of flexible manipulators is to be realized in practical industrial applications.

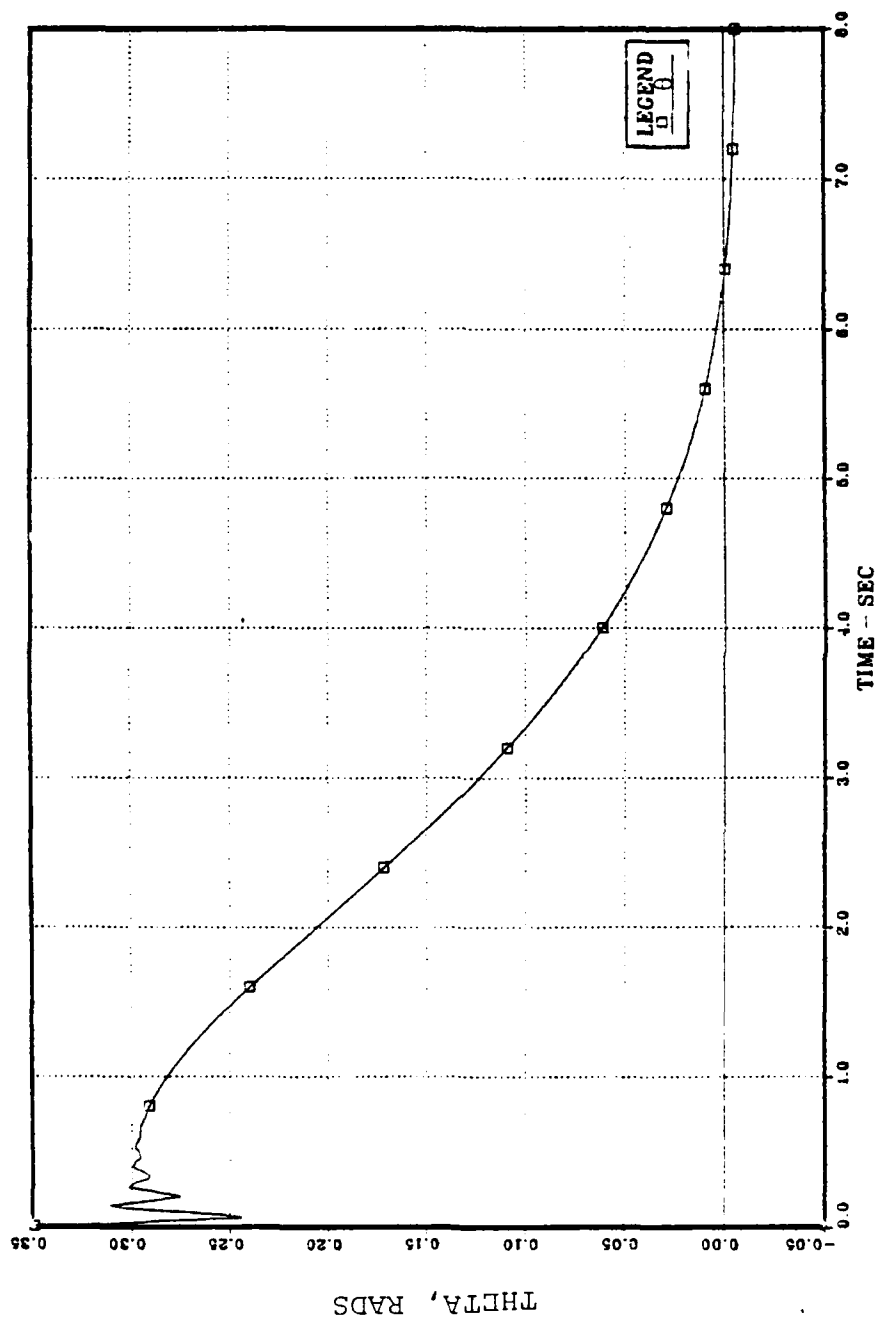


Figure 13. Closed-Loop Response.

VI. CONCLUSIONS

The purpose of this research is to experimentally validate the ERLS dynamic model. The validation of the ERLS dynamic model is needed to ensure confidence of the model for use in future design and control applications. In this research, the ERLS model is tailored to a single-link flexible arm having hydraulic actuation and moving in a vertical plane. The vertical plane motion introduces the effects of gravity. The investigation of the effects of gravity on flexible manipulator movement allows for the consideration of applications not limited to space usage. The investigation of hydraulic power actuation allows for the consideration of heavy load applications. The effects and interactions of modelling the flexible arm with gravity and the hydraulic actuation revealed the importance of proper determination of parameters, specifically those affecting damping.

The acceptable tip position amplitude error despite the single element modelling suggests the ERLS model's potential usefulness in improving the tip position accuracy. This potential benefit is significant considering the importance of tip position accuracy as a criteria for evaluating robot performance.

The results of the validation indicated the theoretical strain and position measurements are affected by the underlying assumptions of the ERLS model. Specifically, the FEM single element modelling of the experimental arm results in a more rigid description of the actual motion and gives smaller amplitudes and higher frequencies. The results indicate that as loading is applied to the single element model the relative percentage errors of the first mode amplitude and frequency increase slightly. As loading is applied, the experimental arm becomes more flexible and the single element model's performance in predicting the first mode motion degrades. The results indicate though that the single element model is better suited for predicting the second mode frequency as the loading is increased. The relative percentage errors for frequency indicate, however, that the single element model better predicts the first mode motion compared to the second mode motion.

The small displacement assumption results in additional error to the theoretical strain and position predictions. This error is most noticeable during the initial stages of the X coordinate tip position motion and increases as the loading increases. The small displacement assumption does not appear to have much effect though, on the strain amplitude and frequency errors as evidenced by the lack of any error increase as the strain is increased by a larger hydraulic excitation current. This conclusion needs to be investigated

for other excitation current values. Other assumptions are made on the values of certain mechanical and hydraulic parameters, particularly inertia properties of the arm and actuator. These assumed values undoubtedly contribute to the error in the theoretical predictions. The agreements and differences between the simulation and the experiment in both arm-tip position and strain measurements provide a valuable validation of the ERLS model. The experimental data serves as a guideline to upgrade the dynamic model, particularly in the validity of the underlying assumptions.

VII. RECOMMENDATIONS

A principal goal in this research is to eventually use the ERLS dynamic model in the design of a complete flexible manipulator system. This system would include a multi-link flexible manipulator and a servo control loop. Two areas of research needed to achieve this goal are, therefore, the control system design and the optimal design of a flexible manipulator.

Continued simulation studies of a closed-loop system having the controller design based on the ERLS model are needed. Alternative control laws need to be investigated for possible use in this application. Concurrent work is needed on the continued validation of the ERLS dynamic model. Specifically, the single element FEM modelling of deformations should be extended to a multi-element model. Validation of the arm and actuator inertia properties needs to be accomplished. The intent of the continued validation of the ERLS dynamic model is to bring the theoretical arm motion into closer agreement to the experimental arm motion. This refinement of the dynamic model is useful for an effective controller design based on the model. Additional techniques for the acquisition of arm tip position need to be investigated and implemented. Specifically, sensors for arm tip position need to be implemented in order to feedback position

data to the controller for appropriate control action. Alternatives for arm tip position sensors include accelerometers and optics. The controller design eventually needs to be implemented in hardware and/or software and tested. Extension of the controller design and implementation to the multi-link case is eventually needed if the advantages of flexible manipulators is to be realized in practical industrial applications.

Once experimental validation is completed the ERLS dynamic model will allow computer simulation for designing a mechanical manipulator with a desired rigidity. Further investigation is needed into the optimal design of a flexible manipulator.

APPENDIX A

DERIVATION OF THE EQUATIONS OF MOTION FOR THE EXPERIMENTAL, SINGLE-LINK, FLEXIBLE ARM

Given the large and small motions as generalized coordinates, the following are the two sets of Lagrange equations used to develop the equations of motion:

$$d/dt(\partial KE/\partial \dot{\theta}) - \partial KE/\partial \theta + \partial PE/\partial \theta = F \quad (A.1)$$

$$d/dt(\partial KE/\partial \dot{U}) - \partial KE/\partial U + \partial PE/\partial U = 0 \quad (A.2)$$

KE - kinetic energy

PE - potential energy

θ - large motion joint variable, theta

U - 2x1 vector of small motion displacement and slope, v
and ϕ

F - generalized force for large motion, applied moment

The actual motion of the experimental arm is restricted to lie in a vertical plane. The hydraulic actuator is attached to the base of the arm. The load is attached to the end of the arm. The large motion joint variable theta is the angle measured between the ERLS link and the global coordinate system horizontal axis.

The origin of the global coordinate system is the axis of the hydraulic actuator, the base joint.

The horizontal and vertical axes of the global coordinate system are parallel and perpendicular to the earth. The ERLS link is parallel to the tangent of the experimental arm at the

base joint. Figure A.1 shows the relationships between the ERLS and the theoretical arm position. The vector of small motion is limited to include only the transverse displacement, v , and the slope, ϕ , of the end of the arm. Axial deformation and torsion are neglected in the model and are considered insignificant in this application. The design of the experimental arm to include two parallel flat bars jointed by a series of transverse bridges makes the arm rigid in torsion. Figure A.1 shows the two components of the vector of small motion.

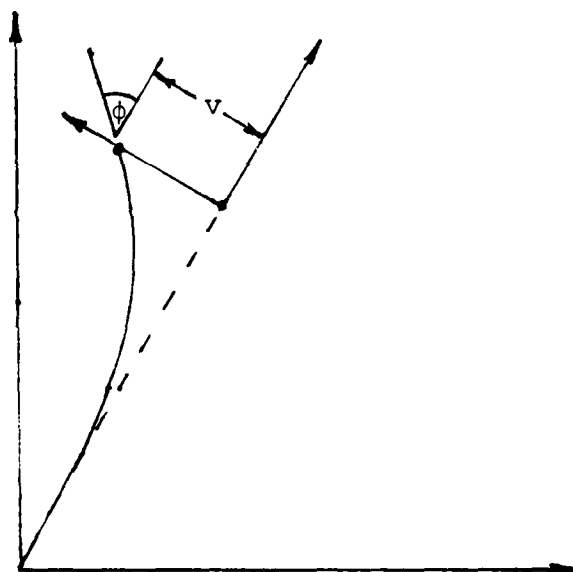


Figure A.1

- - -	ERLS
—	Theoretical Arm Position
X, Y	Global Coordinate System
x, y	Local Coordinate System
v	Arm Tip Deflection
ϕ	Arm Tip Slope

The kinetic energy of the system includes contributions from the arm, the loading and the hydraulic actuator rotor. The expressions utilized for the determination of the kinetic energy of the system are as follows:

$$KE\text{-arm} = 1/2 \int_{\substack{\text{ARM} \\ \text{VOLUME}}} \mu \dot{R}^T (\dot{R}) dv \quad (A.3)$$

$$KE\text{-load} = 1/2 \text{Tr} \int_{\text{LOAD VOLUME}} \mu_1 \dot{R}_1^T (\dot{R}_1) dv \quad (A.4)$$

$$KE\text{-rotor} = 1/2 \text{Tr} \int_{\substack{\text{ROTOR} \\ \text{VOLUME}}} \mu_r \dot{R}_r^T (\dot{R}_r) dv \quad (A.5)$$

Tr is the trace operation.

The global position vector of the arm is determined from the following transformation:

$$R = W (r + D) \quad (A.6)$$

W - the 3x3 transformation matrix and is solely a function of theta

r - the 3x1 local position vector of the arm measured from the coordinate system whose origin is at the end of the ERLS link. Figure A.1 shows the positive directions for the local coordinate system.

D - the 3x1 deformation vector that only includes the transverse displacement, v. In order to introduce the nodal displacements at the arm tip as the sole deformation variables substitution of the shape function matrix and a nodal displacement vector is made for D. The derivation of this substitution is shown in Appendix C.

μ - the mass density of the arm, steel

The global position vector of the load is determined from the following transformation:

$$R_1 = W D_1 r_1 \quad (A.7)$$

D_1 - the 3x3 transformation matrix due to the local deformations of the arm tip

r_1 - the 3x1 local position vector for the load

μ_1 - the mass density of the load, steel

The global position vector of the hydraulic actuator rotor is determined from the following transformation:

$$R_r = A_r r_r \quad (A.8)$$

A_r - the 3x3 transformation matrix due to the large motion rotation of the rotor

r_r - the 3x1 local position vector for the rotor

μ_r - the mass density of the actuator rotor, aluminum

The following definitions for the inertia terms are utilized to simplify the computations and the resultant expressions in the equations of motion:

$$I_1 = \int_{\substack{\text{LOAD} \\ \text{VOLUME}}} \mu_1 r_1 r_1^T dv - \text{the } 3 \times 3 \text{ inertia matrix of the load} \quad (\text{A.9})$$

$$I_r = \int_{\substack{\text{ROTOR} \\ \text{VOLUME}}} \mu_r r_r r_r^T dv - \text{the } 3 \times 3 \text{ inertia matrix of the actuator rotor} \quad (\text{A.10})$$

$$I_{122}(w^T, \ddot{w}_r) = \int_{\substack{\text{LINK} \\ \text{VOLUME}}} \mu \phi_1^T w^T \ddot{w}_r \phi_1 dv \quad (\text{A.11})$$

$$I_{122}(w^T, w) = \int_{\substack{\text{LINK} \\ \text{VOLUME}}} \mu \phi_1^T w^T w \phi_1 dv \quad (\text{A.12})$$

$$I_{121}(w^T, w_\theta) = \int_{\substack{\text{LINK} \\ \text{VOLUME}}} \mu \phi_1^T w^T w_\theta r dv \quad (\text{A.13})$$

$$I_{111}(w_\theta^T, w_\theta) = \int_{\substack{\text{LINK} \\ \text{VOLUME}}} \mu r^T w_\theta^T w_\theta r dv \quad (\text{A.14})$$

$$I_{112}(w_\theta^T, w) = \int_{\substack{\text{LINK} \\ \text{VOLUME}}} \mu r^T w_\theta^T w \phi_1 dv \quad (\text{A.15})$$

$$I_{122}(w_\theta^T, \dot{w}) = \int_{\substack{\text{LINK} \\ \text{VOLUME}}} \mu \phi_1^T w_\theta^T \dot{w} \phi_1 dv \quad (\text{A.16})$$

$$I_{122}(W_{\theta}^T, W_{\theta}) = \int_{\substack{\text{LINK} \\ \text{VOLUME}}} \mu \phi_1^T W_{\theta}^T W_{\theta} \phi_1 dv \quad (\text{A.17})$$

$$I_{YY} = \int_{\substack{\text{LOAD} \\ \text{VOLUME}}} \mu_1 y^2 dv \quad (\text{A.18})$$

$$I_{xx} = \int_{\substack{\text{LOAD} \\ \text{VOLUME}}} \mu_1 x^2 dv \quad (\text{A.19})$$

Computation of the preceding link inertia matrices require utilization of the 3x2 link shape matrix ϕ_1 , the 3x1 link local position vector r , and various combinations of the 3x3 transformation matrix W . The expression W_{θ} implies a derivative with respect to the large motion joint variable, theta. The expression \ddot{W}_r results from a simplification of the second time derivative of the transformation matrix W and is termed a residual acceleration. Further details on the derivation of these expressions can be found in Reference 2 and a listing of these matrices is found in Appendix B in the computer coding.

The potential energy of the system includes contributions from the strain energy of the arm due to deformation and from the gravitational energy of the load and the arm. The expressions utilized for the determination of the potential energy of the system are as follows:

$$PE_d = 1/2 \int_{\substack{\text{LINK} \\ \text{LENGTH}}} E I_{zz} (V'')^2 dx - \text{potential energy due to deformation} \quad (\text{A.20})$$

$$PE_g = - \int_{\substack{\text{LINK} \\ \text{VOLUME}}} \rho r^T g \, dv \quad \begin{array}{l} \text{- potential energy of the link} \\ \text{due to gravitation} \end{array} \quad (A.21)$$

$$PE_{lg} = - \int_{\substack{\text{LOAD} \\ \text{VOLUME}}} \rho_l r_l^T g \, dv \quad \begin{array}{l} \text{- potential energy of the load} \\ \text{due to gravitation} \end{array} \quad (A.22)$$

$E I_{zz}$ - the flexural rigidity in the z direction, or perpendicular to the plane of motion.

v'' - the second derivative of the transverse displacement v with respect to the x local coordinate direction. In order to introduce the nodal displacements at the arm tip as deformation variables substitution of the second derivative of the shape function matrix with respect to the x coordinate direction and a nodal displacement vector is made for v'' . The derivation of this substitution is shown in Appendix C.

g - the gravitational acceleration vector

The following definitions are utilized to simplify the computations and the resultant expressions in the equations of motion:

$$K_{11} = \int_{\substack{\text{LINK} \\ \text{LENGTH}}} r^T C r \, dx \quad \begin{array}{l} \text{- the 2x2 stiffness matrix} \end{array} \quad (A.23)$$

$$H_{11} = \int_{\substack{\text{LINK} \\ \text{VOLUME}}} \rho r^T \, dv \quad \begin{array}{l} \text{- the link first moment of inertia} \\ \text{vector} \end{array} \quad (A.24)$$

$$H_{21} = \int_{\substack{\text{LINK} \\ \text{VOLUME}}} \mu \phi_1^T dv - \text{the link shape matrix first} \\ \text{moment of inertia vector} \quad (\text{A.25})$$

$$H_{41} = \int_{\substack{\text{LOAD} \\ \text{VOLUME}}} \mu_1 r_1^T dv - \text{the load first moment of inertia} \\ \text{vector} \quad (\text{A.26})$$

Γ - the second derivative of the shape function matrix.

C - the 3x3 flexural rigidity matrix including only

$E I_{zz}$.

Substitution of the expressions for kinetic energy and potential energy into the Lagrange equations and after much computation and simplification results in the following two non-linear, coupled, second-order, ordinary, differential equations for the large and small motions of the single-link flexible arm:

$$MQQ \ddot{\theta} + MQN \ddot{U} = FQ \quad (\text{A.27})$$

$$MNQ \ddot{\theta} + MNN \ddot{U} + KN U = FN \quad (\text{A.28})$$

The following are definitions for the coefficients:

$$MQQ = I_{111}(W_{\theta}^T, W_{\theta}) + U^T I_{122}(W_{\theta}^T, W_{\theta}) U + \text{Trace}(W_{\theta} D_1 I_1 \\ D_1^T W_{\theta}^T + A_r I_r A_r^T) \quad (\text{A.29})$$

$$MQN = I_{112}(W_{\theta}^T, W) + ((M_1 L + M_x), (M_x L + I_{xx} + I_{yy})) \quad (\text{A.30})$$

L is the link length. M_x is the first moment of the load with respect to the local coordinate y axis. M_1 is the mass of the load.

$$\begin{aligned} FQ = & 2. U^T I_{122}(W_\theta^T, \dot{W}) \dot{U} + H_{11} W_\theta^T g + U^T H_{21} W_\theta^T g - \\ & \text{Trace}(W_\theta D_1 I_1 D_1^T \ddot{W}_r + 2. W_\theta D_1 I_1 \dot{D}_1^T \dot{W} + A_{r\theta} I_r \ddot{A}_{rr}) + \\ & H_{41} D_1^T W_\theta^T g + T \end{aligned} \quad (A.31)$$

T is the externally applied torque. \ddot{A}_{rr} results from a simplification of the second time derivative of the transformation matrix A_r and is termed a residual acceleration. U is the 2x1 nodal displacement vector containing the link tip deflection, $v(0)$, and slope, $\phi(0)$. The expression $A_{r\theta}$ implies a derivative with respect to the large motion joint variable, theta.

$$\begin{aligned} MNQ = & (\text{Trace}(W_\theta D_1 I_1 D_{11}^T W^T), \text{Trace}(W_\theta D_1 I_1 D_{12}^T W^T)) \\ & + I_{121}(W^T, W_\theta) \end{aligned} \quad (A.32)$$

D_{11} and D_{12} are the derivatives of the arm tip deformation transformation matrix with respect to each nodal displacement, deflection and slope, respectively.

$$MNN = I_{122}(W^T, W) + \begin{bmatrix} M_L & 0 \\ 0 & I_{xx} + I_{yy} \end{bmatrix} \begin{bmatrix} \ddot{v}(0) \\ \ddot{\phi}(0) \end{bmatrix} \quad (A.33)$$

$\ddot{v}(0)$ and $\dot{\phi}(0)$ are arm tip deflection and slope accelerations respectively.

$$KN = K_{11} + I_{122}(W^T, \ddot{W}_r) \quad (A.34)$$

$$\begin{aligned} FN = & H_{21} W^T g - (\text{Trace}(\ddot{W}_r D_1 I_1 D_{11}^T W^T + 2. \dot{W} \dot{D}_1 I_1 D_{11}^T \\ & W^T), \text{Trace}(\ddot{W}_r D_1 I_1 D_{12}^T W^T + 2. \dot{W} \dot{D}_1 I_1 D_{12}^T W^T)) \\ & + (H_{41} D_{11}^T W^T g, H_{41} D_{12}^T W^T g) \end{aligned} \quad (A.35)$$

The numerical values utilized for the experimental flexible arm system variables are listed in Appendix B and are in SI units.

LISTING OF THE FORTRAN CODING UTILIZED IN SOLVING
THE DYNAMIC EQUATIONS OF MOTION FOR THE EXPERIMENTAL
SINGLE-LINK FLEXIBLE ARM

THIS PROGRAM SOLVES THE ERLS FLEXIBLE MANIPULATOR DYNAMICS FOR A SINGLE LINK EXPERIMENTAL ARM. THE EXPERIMENTAL ARM PARAMETERS ARE INPUTTED AND THE HYDRAULIC ACTUATION DYNAMICS ARE INCLUDED IN THE SIMULATION. THE INPUT IS THE CURRENT TO THE SERVOVALVE MOUNTED ON THE HYDRAULIC ACTUATOR AND THE OUTPUT IS THE POSITION OF THE ARM TIP IN THE GLOBAL REFERENCE SYSTEM. THE CODING CONSISTS OF A MAIN PROGRAM AND FIFTEEN SUBROUTINES AND ARE DESCRIBED BELOW.

1. A-EFFECTIVE CROSS-SECTIONAL AREA OF FLEXIBLE ARM
2. ARDD-3X3 SECOND TIME DERIVATIVE OF ROTOR RESIDUAL ACCELERATION MATRIX
3. ARTH-3X3 ROTOR TRANSFORMATION MATRIX DIFFERENTIATED WITH RESPECT TO THETA
4. BE-EFFECTIVE BULK MODULUS OF FLUID
5. BIGF-3X1 RIGHT-HAND SIDE VECTOR FOR LARGE AND SMALL MOTION ACCELERATIONS
6. BIGM-3X3 MATRIX OF LARGE AND SMALL MOTION ACCELERATION COEFFICIENTS
7. CTM-TOTAL LEAKAGE COEFFICIENT OF THE ACTUATOR
8. DEFM-DISPLACEMENT DEFORMATION VARIABLE
9. DEFMD-TIME DERIVATIVE OF DISPLACEMENT DEFORMATION VARIABLE
10. DIFF, QERR, QERR1, FACTOR-DUMMY VARIABLES
11. DL1-3X3 DEFORMATION MATRIX
12. DL11-3X3 DEFORMATION MATRIX DIFFERENTIATED WITH RESPECT TO THE DISPLACEMENT DEFORMATION VARIABLE
13. DL12-3X3 DEFORMATION MATRIX DIFFERENTIATED WITH RESPECT TO THE SLOPE DEFORMATION VARIABLE
14. DL1D-3X3 FIRST TIME DERIVATIVE OF DEFORMATION MATRIX
15. DM-ACTUATOR DISPLACEMENT
16. E-MODULUS OF ELASTICITY OF STEEL
17. FN-2X1 RIGHT-HAND SIDE VECTOR FOR SMALL MOTION ACCELERATIONS
18. FQ-RIGHT-HAND SIDE FOR LARGE MOTION ACCELERATIONS
19. G-3X1 GRAVITATIONAL ACCELERATION VECTOR
20. GPOS-3X1 GLOBAL POSITION VECTOR FOR ARM TIP
21. H11-1X3 LINK FIRST MOMENT OF INERTIA VECTOR
22. H21-2X3 LINK SHAPE MATRIX FIRST MOMENT OF INERTIA VECTOR
23. H41-1X3 LOAD FIRST MOMENT OF INERTIA VECTOR
24. KCE-TOTAL FLOW PRESSURE COEFFICIENT
25. PL-LOAD HYDRAULIC PRESSURE DROP
26. PS-HYDRAULIC SUPPLY PRESSURE
27. QL-FLOW DELIVERED FROM THE SERVOVALVE
28. SLOP-SLOPE DEFORMATION VARIABLE
29. SLOPD-TIME DERIVATIVE OF SLOPE DEFORMATION VARIABLE
30. SOL-3X1 VECTOR OF LARGE AND SMALL MOTION ACCELERATIONS
31. TE-TORQUE EFFICIENCY
32. TH-LARGE MOTION POSITION VARIABLE
33. THD-TIME DERIVATIVE OF LARGE MOTION VARIABLE
34. TORQUE-APPLIED TORQUE BY ACTUATOR
35. U-2X1 ARM TIP DEFORMATION VECTOR INCLUDING DISPLACEMENT AND SLOPE
36. UD-2X1 ARM TIP DEFORMATION VECTOR DIFFERENTIATED WITH RESPECT TO TIME
37. VT-TOTAL COMPRESSED VOLUME INCLUDING ACTUATOR LINES AND CHAMBERS
38. W-3X3 LINK TRANSFORMATION MATRIX
39. WD-3X3 FIRST TIME DERIVATIVE OF LINK TRANSFORMATION MATRIX
40. WRDD-3X3 SECOND TIME DERIVATIVE OF LINK RESIDUAL ACCELERATION MATRIX
41. WTH-3X3 TRANSFORMATION MATRIX DIFFERENTIATED WITH RESPECT TO THETA

```

* VALVE
* 42.XIINP-CURRENT INPUT EQUAL TO INITIAL AND FRACTIONAL AMOUNTS
* 43.XIL-3X3 INERTIA MATRIX OF THE LOAD
* 44.XIO-INITIAL INPUT CURRENT TO SERVOVALVE
* 45.XIR-3X3 ROTOR INERTIA MATRIX
* 46.XISTEP-STEP INPUT OF FRACTIONAL AMOUNT OF INPUT CURRENT
* 47.XK11-2X2 PARTIAL LINK STIFFNESS MATRIX
* 48.XKN-2X2 LINK STIFFNESS MATRIX
* 49.XKV-SERVOVALVE SIZING CONSTANT
* 50.XLL-LENGTH OF FLEXIBLE ARM
* 51.XML-MASS OF LOAD
* 52.XMNN-2X2 COEFFICIENT MATRIX OF SMALL MOTION ACCELERATIONS IN THE
* SMALL MOTION DYNAMIC EQUATIONS
* 53.XMNQ-2X1 COEFFICIENT VECTOR OF LARGE MOTION ACCELERATIONS IN THE
* SMALL MOTION DYNAMIC EQUATIONS
* 54.XMQN-1X2 COEFFICIENT VECTOR OF SMALL MOTION ACCELERATIONS IN THE
* LARGE MOTION DYNAMICS EQUATION
* 55.XMQQ-COEFFICIENT OF LARGE MOTION ACCELERATION IN THE LARGE MOTION
* DYNAMICS EQUATION
* 56.XMQQP-2X2 DUMMY MATRIX FOR USE IN FORMULATING THE EQUATIONS OF
* MOTION
* 57.XMR-MASS OF ACTUATOR ROTOR
* 58.XMU-MASS DENSITY OF STEEL FLEXIBLE ARM
* 59.XMX-FIRST MOMENT OF LOAD WITH RESPECT TO THE LOCAL COORDINATE
* Y AXIS
* 60.XXI-VARIABLE REPRESENTING INERTIA-LIKE LOAD PROPERTY
* 61.YYI-VARIABLE REPRESENTING INERTIA-LIKE LOAD PROPERTY
* 62.ZI-AREA MOMENT OF INERTIA OF FLEXIBLE ARM

```

INITIAL

INITIAL VALUES OF PARAMETERS ARE INPUTTED VIA XINIT SUBROUTINE

```

/ REAL*8 U(2,1),XMQQ(1),XMQQP(2,2),DL1(3,3),WTH(3,3),ARTH(3,3),
/ #XIR(3,3),XMQN(1,2),UD(2,1),H11(1,3),G(3,1),H21(2,3),
/ #WRDD(3,3),DL1D(3,3),WD(3,3),ARRDD(3,3),H41(1,3),XK11(2,2),
/ #DL12(3,3),XMNQ(2,1),W(3,3),XMNN(2,2),XKN(2,2),FN(2,1),BIGM(3,3),
/ #BIGF(3,1),XIL(3,3),DL11(3,3),DEFMD(1),SOL(3),THD(1),SLOP(1),
/ #SLOPD(1),A(1),E(1),ZI(1),XXI(1),YYI(1),FQ(1),GPOS(3),XITH(1),
/ #XMU(1),XLL(1),XML(1),XMR(1),XMX(1),TH(1),TORQUE(1),DEFM(1),
/ #PS(1),XIFRAC(1),XIO(1),KCE(1),VT(1),BE(1),DM(1),XKV(1),TE(1),
/ #QL(1),PL(1),DIFF(1),XIINP(1),QERRI(1),QERR(1),FACTOR(1),XISTEP(1)
FIXED I
NOSORT
SYSTEM DPINTG

```

4TH ORDER RUNGE-KUTTA DOUBLE-PRECISION INTEGRATION

METHOD RKSDP

INITIALIZATION SUBROUTINE

```

CALL XINIT(TH,THD,DEFM,DEFMD,SLOP,SLOPD,VO,PJSD,A,XML,XMU,...
XLL,XMR,E,ZI,PS,XIFRAC,XIO,CIM,VT,BE,DM,XKV,TE,QL,...
PL,PLIC)

```

DYNAMIC

COEFFICIENTS FOR BOTH LARGE AND SMALL MOTION ACCELERATIONS AND THE RIGHT-HAND SIDES ARE COMPUTED IN THE FOLLOWING SUBROUTINES. ALSO, THE HYDRAULIC DYNAMICS ARE INCLUDED IN THE MAIN PROGRAM.

NOSORT

```

*      HYDRAULIC DYNAMICS
*
XISTEP(1)=XIFRAC(1)*STEP(0.0)
XIINP(1)=XIO(1)+XISTEP(1)
IF(PL(1).GT.PS(1)) GO TO 2
GO TO 3
2  PL(1)=PS(1)
3  QERR1(1)=(XIINP(1)*XKV(1)*DSQRT(P(1)-PL(1)))-(DM(1)*THD(1))
   QERR(1)=QERR1(1)/KCE(1)
   DIFF(1)=QERR(1)-PL(1)
   FACTOR(1)=VT(1)/(4.0D0*BE(1)*KCE(1))
   DIFF1(1)=DIFF(1)
   SORT
   PL1=INTGRL(PLIC,DIFF1,1)
   NOSORT
   PL(1)=PL1(1)/FACTOR(1)
   TORQUE(1)=TE(1)*PL(1)*DM(1)
*
*      MATRIX AND VECTOR FORMULATION SUBROUTINE
*
CALL FORM(W, WTH, WD, DL1, DL1D, XIL, XIR, ARTH, WRDD, ARRDD, U, UD, ...
XMQQP, G, H11, H21, DL11, DL12, H41, XK11, A, XMU, XML, XLL, TH, THD, ...
DEFM, DEFMD, SLOP, SLOPD, E, ZI, XMR, XMX, YYI, XXI)
*
*      COEFFICIENT OF LARGE MOTION ACCELERATION IN LARGE MOTION DYNAMICS
*      EQUATION SUBROUTINE
*
CALL XLMMQQ(XMQQ, U, XMQQP, DL1, WTH, ARTH, XIL, XIR, A, XMU, TH, DEFM, SLOP)
*
*      COEFFICIENTS OF SMALL MOTION ACCELERATIONS IN LARGE MOTION DYNAMICS
*      EQUATION SUBROUTINE
*
CALL XLMMQN(XMQN, A, XMU, XML, XLL, XMX, SLOP, DEFM, YYI, XXI)
*
*      RIGHT-HAND SIDE FOR LARGE MOTION DYNAMICS EQUATION SUBROUTINE
*
CALL XLMFQ(FQ, U, XMQQP, DL1, WTH, ARTH, XIL, XIR, UD, H11, G, H21, WRDD, ...
DL1D, WD, ARRDD, H41, TH, THD, DEFM, DEFMD, SLOP, SLOPD, A, XMU, XML, XLL, ...
TORQUE)
*
*      LINK STIFFNESS MATRIX SUBROUTINE
*
CALL SMKN(XKN, XK11, XMQQP, A, XMU, THD)
*
*      COEFFICIENTS OF LARGE MOTION ACCELERATION IN SMALL MOTION
*      DYNAMICS EQUATIONS SUBROUTINE
*
CALL SMMNQ(XMNQ, DL1, WTH, XIL, DL11, DL12, W, TH, DEFM, SLOP, A, XMU)
*
*      RIGHT-HAND SIDE OF SMALL MOTION DYNAMICS EQUATIONS SUBROUTINE
*
CALL SMFN(FN, H21, W, G, WRDD, DL1, XIL, DL11, DL12, WD, DL1D, H41, TH, ...
THD, DEFM, DEFMD, SLOP, SLOPD)
*
*      COEFFICIENTS OF SMALL MOTION ACCELERATIONS IN SMALL MOTION DYNAMICS
*      EQUATIONS SUBROUTINE
*
CALL SMMNN(XMNN, XMQQP, XML, A, XMU, XXI, YYI, XMX)
*
*      ACCELERATION COEFFICIENTS MATRIX AND RIGHT-HAND SIDE VECTOR
*      FORMULATION SUBROUTINE
*
CALL BIGFOR(BIGM, BIGF, XMQQ, XMQN, FQ, XMNQ, XMNN, XKN, FN, U)
*
*      LINEAR EQUATION SOLVER FOR ACCELERATIONS SUBROUTINE
*
CALL XLEQ(BIGM, BIGF, SOL)
*
*      TRANSFORMATION FROM LOCAL COORDINATE TO GLOBAL COORDINATE TIP
*      POSITION SUBROUTINE
*
CALL GLOB(GPOS, W, DEFM)

```



```

BE=690.D6
A=6.17795D-04
ML=.423300000000000
MU=7861.05000000000000
LL=0.998500000000000
MR=9.00011451000000
E=2.0D11
ZI=4.065D-10
VO(1)=0.000000000000000
VO(2)=0.000000000000000
VO(3)=0.000000000000000
POSO(1)=0.000000000000000
POSO(2)=-.07804116400000
POSO(3)=-.09875534300000
TH=POSO(1)
THD=VO(1)
DEFM=POSO(2)
DEFMD=VO(2)
SLOP=POSO(3)
SLOPD=VO(3)
RETURN
END

```

C
C
C

```

SUBROUTINE FORM(W,WTH,WD,DL1,DL1D,XIL,XIR,ARTH,WRDD,ARRDD,U,UD,
#XMQQP,G,H11,H21,DL11,DL12,H41,XK11,A,MU,ML,LL,TH,THD,DEFM,DEFMD,
#SLOP,SLOPD,E,ZI,MR,MX,YYI,XXI)
REAL*8 W(3,3),WTH(3,3),WD(3,3),DL1(3,3),DL1D(3,3),XIL(3,3)
REAL*8 XIR(3,3),ARTH(3,3),WRDD(3,3),ARRDD(3,3),U(2,1),UD(2,1)
REAL*8 XMQQP(2,2),G(3,1),H11(1,3),H21(2,3),DL11(3,3),DL12(3,3)
REAL*8 H41(1,3),XK11(2,2),MU,ML,LL,MR,MX,TH
REAL*8 THD,DEFM,DEFMD,SLOP,SLOPD,XXI,YYI,A,E,ZI
W(1,1)=1.000000000000000
W(1,2)=0.000000000000000
W(1,3)=0.000000000000000
W(2,1)=LL*DCOS(TH)
W(2,2)=DCOS(TH)
W(2,3)=-DSIN(TH)
W(3,1)=LL*DSIN(TH)
W(3,2)=DSIN(TH)
W(3,3)=DCOS(TH)
WTH(1,1)=0.000000000000000
WTH(1,2)=0.000000000000000
WTH(1,3)=0.000000000000000
WTH(2,1)=-LL*DSIN(TH)
WTH(2,2)=-DSIN(TH)
WTH(2,3)=-DCOS(TH)
WTH(3,1)=LL*DCOS(TH)
WTH(3,2)=DCOS(TH)
WTH(3,3)=-DSIN(TH)
WD(1,1)=0.000000000000000
WD(1,2)=0.000000000000000
WD(1,3)=0.000000000000000
WD(2,1)=-LL*DSIN(TH)*THD
WD(2,2)=-DSIN(TH)*THD
WD(2,3)=-DCOS(TH)*THD
WD(3,1)=LL*DCOS(TH)*THD
WD(3,2)=DCOS(TH)*THD
WD(3,3)=-DSIN(TH)*THD
DL1(1,1)=1.000000000000000
DL1(1,2)=0.000000000000000
DL1(1,3)=0.000000000000000
DL1(2,1)=0.000000000000000
DL1(2,2)=1.000000000000000
DL1(2,3)=-SLOP
DL1(3,1)=DEFM
DL1(3,2)=SLOP
DL1(3,3)=1.000000000000000
DL1D(1,1)=0.000000000000000
DL1D(1,2)=0.000000000000000
DL1D(1,3)=0.000000000000000

```

```

DL1D(2,1)=0.00000000000000
DL1D(2,2)=0.00000000000000
DL1D(2,3)=-SLOPD
DL1D(3,1)=DEFMD
DL1D(3,2)=SLOPD
DL1D(3,3)=0.00000000000000
XIL(1,1)=ML
XIL(1,2)=0.00067141800000
XIL(1,3)=0.00000000000000
XIL(2,1)=0.00067141800000
XIL(2,2)=1.422D-06
XIL(2,3)=0.00000000000000
XIL(3,1)=0.00000000000000
XIL(3,2)=0.00000000000000
XIL(3,3)=5.97754D-04
MX=0.00067141800000
XXI=1.422D-06
YYI=5.97754D-04
XIR(1,1)=MR
XIR(1,2)=0.00000000000000
XIR(1,3)=0.00000000000000
XIR(2,1)=0.00000000000000
XIR(2,2)=0.02746713000000
XIR(2,3)=0.00000000000000
XIR(3,1)=0.00000000000000
XIR(3,2)=0.00000000000000
XIR(3,3)=0.02746713000000
ARTH(1,1)=0.00000000000000
ARTH(1,2)=0.00000000000000
ARTH(1,3)=0.00000000000000
ARTH(2,1)=0.00000000000000
ARTH(2,2)=-DSIN(TH)
ARTH(2,3)=-DCOS(TH)
ARTH(3,1)=0.00000000000000
ARTH(3,2)=DCOS(TH)
ARTH(3,3)=-DSIN(TH)
WRDD(1,1)=0.00000000000000
WRDD(1,2)=0.00000000000000
WRDD(1,3)=0.00000000000000
WRDD(2,1)=-LL*DCOS(TH)*(THD**2)
WRDD(2,2)=-DCOS(TH)*(THD**2)
WRDD(2,3)=DSIN(TH)*(THD**2)
WRDD(3,1)=-LL*DSIN(TH)*(THD**2)
WRDD(3,2)=-DSIN(TH)*(THD**2)
WRDD(3,3)=-DCOS(TH)*(THD**2)
ARRDD(1,1)=0.00000000000000
ARRDD(1,2)=0.00000000000000
ARRDD(1,3)=0.00000000000000
ARRDD(2,1)=0.00000000000000
ARRDD(2,2)=-DCOS(TH)*(THD**2)
ARRDD(2,3)=DSIN(TH)*(THD**2)
ARRDD(3,1)=0.00000000000000
ARRDD(3,2)=-DSIN(TH)*(THD**2)
ARRDD(3,3)=-DCOS(TH)*(THD**2)
U(1,1)=DEFM
U(2,1)=SLOP
UD(1,1)=DEFMD
UD(2,1)=SLOPD
XMQQP(1,1)=.37142860000000
XMQQP(1,2)=-.05238100000000
XMQQP(2,1)=-.05238100000000
XMQQP(2,2)=.00952380000000
G(1,1)=0.00000000000000
G(2,1)=0.00000000000000
G(3,1)=-9.80660000000000
H11(1,1)=4.85651900000000
H11(1,2)=-2.42825869300000
H11(1,3)=0.00000000000000
H21(1,1)=0.00000000000000
H21(1,2)=0.00000000000000
H21(1,3)=A*MU*(.50000000000000)
H21(2,1)=0.00000000000000

```

```

H21(2,2)=0.000000000000000
H21(2,3)=A*MU*(-.083333333333333)
DO 50 I=1,3
DO 60 J=1,3
DL11(I,J)=0.000000000000000
DL12(I,J)=0.000000000000000
60 CONTINUE
50 CONTINUE
DL11(3,1)=1.000000000000000
DL12(2,3)=-1.000000000000000
DL12(3,2)=1.000000000000000
H41(1,1)=ML
H41(1,2)=0.000671418000000
H41(1,3)=.00000000000000000
XK11(1,1)=12.000000000000000*E*ZI
XK11(1,2)=-6.000000000000000*E*ZI
XK11(2,1)=-6.000000000000000*E*ZI
XK11(2,2)=4.000000000000000*E*ZI
RETURN
END

```

C
C
C

```

SUBROUTINE XLMMQQ(MQQ,U,XMQQP,DL1,WTH,ARTH,XIL,XIR,A,MU,TH,DEFM,
#SLOP)
REAL*8 MQQ,UT(1,2),P(1,2),DL1T(3,3),WTHT(3,3),ARTHT(3,3),P1(3,3)
REAL*8 P2(3,3),P3(3,3),P4(3,3),P5(3,3),P6(3,3),P7(3,3),MU
REAL*8 U(2,1),XMQQP(2,2),DL1(3,3),WTH(3,3),ARTH(3,3),XIL(3,3)
REAL*8 XIR(3,3),A,TH,DEFM,SLOP,SP,TP
M=2
L=1
N=3
MQQ=0.000000000000000
CALL TRANS(U,UT,M,L)
CALL MATMUL(UT,XMQQP,L,M,M,P)
CALL MATMUL(P,U,L,M,L,SP)
CALL TRANS(DL1,DL1T,N,N)
CALL TRANS(ARTH,ARTHT,N,N)
CALL TRANS(WTH,WTHT,N,N)
CALL MATMUL(WTH,DL1,N,N,N,P1)
CALL MATMUL(P1,XIL,N,N,N,P2)
CALL MATMUL(P2,DL1T,N,N,N,P3)
CALL MATMUL(P3,WTHT,N,N,N,P4)
CALL MATMUL(ARTH,XIR,N,N,N,P5)
CALL MATMUL(P5,ARTHT,N,N,N,P6)
CALL MATADD(P4,P6,N,N,P7)
CALL TRACE(P7,N,TP)
MQQ=((1./3.)*A*MU) + (A*MU*SP) + TP
RETURN
END

```

C
C
C

```

SUBROUTINE XLMMQN(XMQN,A,MU,ML,LL,MX,SLOP,DEFM,YYI,XXI)
REAL*8 XMQN(1,2),MU,ML,LL,MX,A,SLOP,DEFM,YYI,XXI
XMQN(1,1)=(A*MU*(.350000000000000))+(ML*LL)+MX
XMQN(1,2)=(A*MU*(-.050000000000000))+(MX*LL)+YYI+XXI
RETURN
END

```

C
C
C

```

SUBROUTINE XLMFQ(FQ,U,XMQQP,DL1,WTH,ARTH,XIL,XIR,UD,H11,G,H21,
#WRDD,DL1D,WD,ARRDD,H41,TH,THD,DEFM,DEFMD,SLOP,SLOPD,A,MU,ML,LL,
#TORQUE)
REAL*8 FQP(2,2),P(1,2),P1(1,3),P2(1,3),P3(1,3),P4(3,3),P5(3,3)
REAL*8 P6(3,3),P7(3,3),P8(3,3),P9(3,3),P10(3,3),P11(1,3),P12(1,3)
REAL*8 FPFH(3,3),FHP(3,3),FPT(3,3),DL1DT(3,3),WDT(3,3),ARRDDT(3,3)
REAL*8 UT(1,2),DL1T(3,3),WRDDT(3,3),FPF(3,3),FPS(3,3),WTHT(3,3)
REAL*8 U(2,1),XMQQP(2,2),DL1(3,3),WTH(3,3),ARTH(3,3),XIL(3,3)
REAL*8 XIR(3,3),UD(2,1),H11(1,3),G(3,1),H21(2,3),WRDD(3,3)
REAL*8 DL1D(3,3),WD(3,3),ARRDD(3,3),H41(1,3),MU,LL,ML

```



```

REAL*8 A,TORQUE,FQ,TH,THD,DEFM,DEFMD,SLOP,SLOPD
REAL*8 FP,SP,TP,TFP,FTHP
M=2
L=1
N=3
CALL TRANS(U,UT,M,L)
DO 10 I=1,2
DO 20 J=1,2
FQP(I,J)=XMQQP(I,J)*THD
20 CONTINUE
10 CONTINUE
CALL MATMUL(UT,FQP,L,M,M,P)
CALL MATMUL(P,UD,L,M,L,FP)
CALL TRANS(WTH,WTHT,N,N)
CALL MATMUL(H11,WTHT,L,N,N,P1)
CALL MATMUL(P1,G,L,N,L,SP)
CALL MATMUL(UT,H21,L,M,N,P2)
CALL MATMUL(P2,WTHT,L,N,N,P3)
CALL MATMUL(P3,G,L,N,L,TP)
CALL TRANS(DL1,DL1T,N,N)
CALL TRANS(WRDD,WRDDT,N,N)
CALL MATMUL(WTH,DL1,N,N,N,P4)
CALL MATMUL(P4,XIL,N,N,N,P5)
CALL MATMUL(P5,DL1T,N,N,N,P6)
CALL MATMUL(P6,WRDDT,N,N,N,FPF)
CALL TRANS(DL1D,DL1DT,N,N)
CALL TRANS(WD,WDT,N,N)
CALL MATMUL(WTH,DL1,N,N,N,P7)
CALL MATMUL(P7,XIL,N,N,N,P8)
CALL MATMUL(P8,DL1DT,N,N,N,P9)
CALL MATMUL(P9,WDT,N,N,N,FPS)
CALL TRANS(ARRDD,ARRDDT,N,N)
CALL MATMUL(ARTH,XIR,N,N,N,P10)
CALL MATMUL(P10,ARRDDT,N,N,N,FPT)
DO 30 I=1,3
DO 40 J=1,3
FPS(I,J)=FPS(I,J)*2.
40 CONTINUE
30 CONTINUE
CALL MATADD(FPF,FPS,N,N,FPFH)
CALL MATADD(FPFH,FPT,N,N,FHP)
CALL TRACE(FHP,N,TFP)
CALL MATMUL(H41,DL1T,L,N,N,P11)
CALL MATMUL(P11,WTHT,L,N,N,P12)
CALL MATMUL(P12,G,L,N,L,FTHP)
FQ=(-2.*A*MU*FP) + SP + TP - TFP + FTHP + TORQUE
RETURN
END

C
C
C
SUBROUTINE SMKN(XKN,XK11,XMQQP,A,MU,THD)
REAL*8 XKN(2,2),KNP(2,2),XMQQP(2,2),XK11(2,2),A,THD,MU
DO 10 I=1,2
DO 20 J=1,2
KNP(I,J)=XMQQP(I,J)*(-A)*MU*(THD**2)
XKN(I,J)=KNP(I,J)+XK11(I,J)
20 CONTINUE
10 CONTINUE
RETURN
END

C
C
C
SUBROUTINE SMMNQ(XMNQ,DL1,WTH,XIL,DL11,DL12,W,TH,DEFM,SLOP,A,MU)
REAL*8 XMNQ(2,1),DL12T(3,3),DL11T(3,3),WT(3,3),P1(3,3),P2(3,3)
REAL*8 P3(3,3),P4(3,3),P5(3,3),P6(3,3),DL1(3,3),WTH(3,3),XIL(3,3)
REAL*8 W(3,3),DL11(3,3),DL12(3,3),TH,DEFM,SLOP,A,MU
M=2
L=1
N=3
CALL TRANS(DL11,DL11T,N,N)

```

```

CALL TRANS(DL12,DL12T,N,N)
CALL TRANS(W,WT,N,N)
CALL MATMUL(WTH,DL1,N,N,N,P1)
CALL MATMUL(P1,XIL,N,N,N,P2)
CALL MATMUL(P2,DL11T,N,N,N,P3)
CALL MATMUL(P3,WT,N,N,N,P4)
CALL TRACE(P4,N,TFP1)
XMNQ(1,1)=TFP1 + ((.350000000000000)*A*MU)
CALL MATMUL(P2,DL12T,N,N,N,P5)
CALL MATMUL(P5,WT,N,N,N,P6)
CALL TRACE(P6,N,TFP2)
XMNQ(2,1)=TFP2 + (-.050000000000000)*A*MU)
RETURN
END

```

C
C
C

```

SUBROUTINE SMFN(FN,H21,W,G,WRDD,DL1,XIL,DL11,DL12,WD,DL1D,H41,TH,
*THD,DEFM,DEFMD,SLOP,SLOPD)
REAL*8 FN(2,1),P1(2,3),P2(3,3),P3(3,3),P4(3,3),P5(3,3),P6(3,3)
REAL*8 P7(3,3),P8(3,3),P9(3,3),P10(3,3),P11(3,3),P12(3,3),P13(3,3)
REAL*8 P14(1,3),P15(1,3),P16(1,3),P17(1,3),TP(2,1),FP(2,1),SP(2,1)
REAL*8 FN1(3,3),FN2(3,3),G(3,1),H21(2,3),WRDD(3,3),DL1D(3,3)
REAL*8 WD(3,3),H41(1,3),XIL(3,3),W(3,3),DL11(3,3),DL12(3,3)
REAL*8 DL1(3,3),DL11T(3,3),DL12T(3,3),WT(3,3)
REAL*8 TH,THD,DEFM,DEFMD,SLOP,SLOPD
M=2
L=1
N=3
CALL TRANS(W,WT,N,N)
CALL MATMUL(H21,WT,M,N,N,P1)
CALL MATMUL(P1,G,M,N,L,FP)
CALL TRANS(DL11,DL11T,N,N)
CALL TRANS(DL12,DL12T,N,N)
CALL MATMUL(WRDD,DL1,N,N,N,P2)
CALL MATMUL(P2,XIL,N,N,N,P3)
CALL MATMUL(P3,DL11T,N,N,N,P4)
CALL MATMUL(P4,WT,N,N,N,P5)
CALL MATMUL(WD,DL1D,N,N,N,P6)
CALL MATMUL(P6,XIL,N,N,N,P7)
CALL MATMUL(P7,DL11T,N,N,N,P8)
CALL MATMUL(P8,WT,N,N,N,P9)
CALL MATMUL(P3,DL12T,N,N,N,P10)
CALL MATMUL(P10,WT,N,N,N,P11)
CALL MATMUL(P7,DL12T,N,N,N,P12)
CALL MATMUL(P12,WT,N,N,N,P13)
DO 10 I=1,3
DO 20 J=1,3
P9(I,J)=P9(I,J)*2.
P13(I,J)=P13(I,J)*2.
20 CONTINUE
10 CONTINUE
CALL MATADD(P5,P9,N,N,FN1)
CALL MATADD(P11,P13,N,N,FN2)
CALL TRACE(FN1,N,TFN1)
CALL TRACE(FN2,N,TFN2)
SP(1,1)=TFN1
SP(2,1)=TFN2
CALL MATMUL(H41,DL11T,L,N,N,P14)
CALL MATMUL(P14,WT,L,N,N,P15)
CALL MATMUL(P15,G,L,N,L,FN3)
CALL MATMUL(H41,DL12T,L,N,N,P16)
CALL MATMUL(P16,WT,L,N,N,P17)
CALL MATMUL(P17,G,L,N,L,FN4)
TP(1,1)=FN3
TP(2,1)=FN4
DO 31 I=1,2
FN(I,1)=FP(I,1) - SP(I,1) + TP(I,1)
31 CONTINUE
RETURN
END

```

C

```

C
C
SUBROUTINE SMMNN(XMNN,XMQQP,ML,A,MU,XXI,YYI,MX)
REAL*8 XMNN(2,2),XMQQP(2,2),ML,MU,A,XXI,YYI,MX
DO 10 I=1,2
DO 20 J=1,2
XMNN(I,J)=0.0000000000000000
20 CONTINUE
10 CONTINUE
XMNN(1,1)=ML
XMNN(1,2)=MX
XMNN(2,1)=MX
XMNN(2,2)=XXI+YYI
DO 30 I=1,2
DO 40 J=1,2
XMNN(I,J)=XMNN(I,J) + XMQQP(I,J)*A*MU
40 CONTINUE
30 CONTINUE
RETURN
END

```

```

C
C
C      MATRIX MULTIPLICATION SUBROUTINE
SUBROUTINE MATMUL(A,B,M,L,N,C)
REAL*8 A(M,L),B(L,N),C(M,N)
DO 10 I=1,M
DO 20 J=1,N
C(I,J)=0.0
DO 30 INDEX=1,L
C(I,J)=C(I,J) + A(I,INDEX)*B(INDEX,J)
30 CONTINUE
20 CONTINUE
10 CONTINUE
RETURN
END

```

```

C
C
C      MATRIX TRANSPOSE SUBROUTINE
SUBROUTINE TRANS(A,B,M,L)
REAL*8 A(M,L),B(L,M)
DO 10 I=1,M
DO 20 J=1,L
B(J,I)=A(I,J)
20 CONTINUE
10 CONTINUE
RETURN
END

```

```

C
C
C      MATRIX TRACE SUBROUTINE
SUBROUTINE TRACE(A,M,TRAC)
REAL*8 A(M,M)
TRAC=0.0
DO 10 I=1,M
TRAC=TRAC + A(I,I)
10 CONTINUE
RETURN
END

```

```

C
C
C      MATRIX ADDITION SUBROUTINE
SUBROUTINE MATADD(A,B,M,L,C)
REAL*8 A(M,L),B(M,L),C(M,L)
DO 10 I=1,M
DO 20 J=1,L
C(I,J)=A(I,J) + B(I,J)
20 CONTINUE
10 CONTINUE
RETURN
END

```

```

C
C

```

```

C
SUBROUTINE BIGFOR(BIGM,BIGF,MQQ,XMQN,FQ,XMNQ,XMNN,XKN,FN,U)
REAL*8 BIGM(3,3),BIGF(3,1),XMQN(1,2),XMNQ(2,1),XMNN(2,2),XKN(2,2)
REAL*8 FN(2,1),U(2,1),MQQ,P(2,1),FQ
M=2
L=1
BIGM(1,1)=MQQ
BIGM(1,2)=XMQN(1,1)
BIGM(1,3)=XMQN(1,2)
BIGM(2,1)=XMNQ(1,1)
BIGM(2,2)=XMNN(1,1)
BIGM(2,3)=XMNN(1,2)
BIGM(3,1)=XMNQ(2,1)
BIGM(3,2)=XMNN(2,1)
BIGM(3,3)=XMNN(2,2)
BIGF(1,1)=FQ
CALL MATMUL(XKN,U,M,M,L,P)
BIGF(2,1)=FN(1,1)-P(1,1)
BIGF(3,1)=FN(2,1)-P(2,1)
RETURN
END

C
C
C
SUBROUTINE XLEQ(BIGM,BIGF,SOL)
REAL*8 BIGM(3,3),BIGF(3,1),SOL(3),WKAREA(18)
M=1
N=3
CALL LEQT2F (BIGM,M,N,N,BIGF,M,WKAREA,IER)
DO 10 I=1,3
SOL(I)=BIGF(I,1)
10 CONTINUE
RETURN
END

C
C
C
SUBROUTINE GLOB(GPOS,W,DEFM)
REAL*8 GPOS(3),W(3,3),DEFM,RL(3)
RL(1)=1.0D0
RL(2)=0.0D0
RL(3)=DEFM
N=3
L=1
CALL MATMUL(W,RL,N,N,L,GPOS)
RETURN
END

ENDJOB
/*
//

```

APPENDIX C

DERIVATION OF THE SHAPE FUNCTION MATRIX AND THE NODAL DISPLACEMENT VECTOR

A cubic shape function is assumed to represent the transverse displacement of the single link flexible arm as follows,

$$v = a_0 + a_1 x + a_2 x^2 + a_3 x^3 \quad - \text{displacement} \quad (\text{C.1})$$

$$\phi = a_1 + 2. a_2 x + 3. a_3 x^2 \quad - \text{slope} \quad (\text{C.2})$$

The boundary conditions of zero displacement and slope at the base where x is equal to minus the link length, L , is invoked. This is in accordance with the positive sign convention of the local coordinate system.

Substituting the boundary conditions into the shape functions gives,

$$v(-L) = a_0 - a_1 L + a_2 L^2 - a_3 L^3 = 0 \quad (\text{C.3})$$

$$\phi(-L) = a_1 - 2. a_2 L + 3. a_3 L^2 = 0 \quad (\text{C.4})$$

$$v(0) = a_0 \quad (\text{C.5})$$

$$\phi(0) = a_1 \quad (\text{C.6})$$

Substituting (C.5) and (C.6) into (C.3) and (C.4) and solving the two equations for a_2 and a_3 gives:

$$a_2 = (2. \phi(0) L - 3. v(0))/L^2 \quad (\text{C.7})$$

$$a_3 = (\phi(0) L - 2. v(0))/L^3 \quad (\text{C.8})$$

Substituting (C.5), (C.6), (C.7), (C.8) into (C.1) and collecting terms gives an expression for the transverse displacement along the arm length as a function of the arm tip nodal displacements, $v(0)$ and $\phi(0)$,

$$v(x) = 1. - (3. x^2)/L^2 - (2. x^3)/L^3) v(0) + (x + (2. x^2)/L + (x^3)/L^2) \phi(0) \quad (C.9)$$

Substituting $v(x)$ into the 3x1 deformation vector results in a 3x2 shape function matrix and a 2x1 nodal displacement vector as follows,

$$D = (0, 0, v(x))^T \begin{bmatrix} 0 & 0 \\ 0 & 0 \\ (1 - \frac{3x^2}{L^2} - \frac{2x^3}{L^3}) & (x + \frac{2x^2}{L} + \frac{x^3}{L^2}) \end{bmatrix} (v(0), \phi(0))^T \quad (C.10)$$

Since the expression v'' is necessary for determining the potential energy due to deformation, the shape function matrix is differentiated twice and results in the following modified shape function matrix.

$$(0, 0, v'')^T \begin{bmatrix} 0 & 0 \\ 0 & 0 \\ (-\frac{6}{L^2} - \frac{12x}{L^3}) & (\frac{4}{L} + \frac{6x}{L^2}) \end{bmatrix} (v(0), \phi(0)) \quad (C.11)$$

The theoretical strain is computed from the expression for v'' obtained from the modified shape function matrix. Assuming simple beam theory, v'' is approximated to equal the curvature, and since curvature is related to strain, the following expression is obtained for the strain:

$$\epsilon_m = c_1 v'' \quad (C.12)$$

ϵ_m is the strain at the maximum distance from the neutral axis

c_1 is the maximum distance from the neutral axis

APPENDIX D

LINEARIZATION, STATE SPACE REPRESENTATION, AND OPTIMAL CONTROLLER DESIGN OF SINGLE-LINK DYNAMIC EQUATIONS (ERLS)

The equations of motion for the single-link flexible arm were defined as follows:

$$MQQ \ddot{\theta} + MQN \ddot{U} = F \quad (D.1)$$

$$MNQ \ddot{\theta} + MNN \ddot{U} + KN U = FN \quad (D.2)$$

The linearized operating point is defined as follows:

$$U = 0.0 \quad \theta = 0.0 \quad (D.3)$$

$$\dot{U} = 0.0 \quad \dot{\theta} = 0.0$$

$$\ddot{U} = 0.0 \quad \ddot{\theta} = 0.0$$

Taking the differential of each coefficient and term in the equations of motion and evaluating them at the operating point gives the following two linearized equations of motion.

$$F_1 \ddot{\theta} + F_2 \ddot{U} = T \quad (D.4)$$

$$F_3 \ddot{\theta} + F_4 \ddot{U} + F_5 U = 0.0 \quad (D.5)$$

where the coefficients are the linearized complements of the non-linear coefficients as follows:

F_1 is from MQQ , F_2 is from MQN , and T is the applied torque.

F_3 is from MNQ , F_4 is from MNN , and F_5 is from KN .

The state space variables are defined as follows:

$$\begin{aligned} x_1 &= \theta & x_2 &= \dot{\theta} \\ x_3 &= \dot{U} & x_4 &= \ddot{U} \\ x_5 &= U & x_6 &= \dot{U} \end{aligned} \quad (D.6)$$

Utilizing equations (D.3) through (D.5) and the state variable description, the following 6x6 matrix equation is formed:

$$\begin{bmatrix} 0 & F_1 & F_2 & 0 & 0 \\ & & 1 \times 2 & & \\ 0 & F_3 & F_4 & 0 & 0 \\ & 2 \times 1 & 2 \times 2 & & \\ 1 & 0 & 0 & 0 & 0 \\ 0 & 0 & 0 & 0 & 1 \\ 0 & 0 & 0 & 0 & 1 \end{bmatrix} \begin{bmatrix} \dot{x}_1 \\ \dot{x}_2 \\ \dot{x}_3 \\ \dot{x}_4 \\ \dot{x}_5 \\ \dot{x}_6 \end{bmatrix} = \begin{bmatrix} 0 & 0 & 0 & 0 & 0 & 0 \\ 0 & 0 & 0 & 0 & -F_5 & \\ 0 & 0 & 0 & 0 & 2 \times 2 & \\ 0 & 1 & 0 & 0 & 0 & 0 \\ 0 & 0 & 1 & 0 & 0 & 0 \\ 0 & 0 & 0 & 1 & 0 & 0 \end{bmatrix} \begin{bmatrix} x_1 \\ x_2 \\ x_3 \\ x_4 \\ x_5 \\ x_6 \end{bmatrix} + \begin{bmatrix} 1 \\ 0 \\ 0 \\ 0 \\ 0 \\ 0 \end{bmatrix} T$$

M
F
 T_1

(D.7)

Equation (D.7) is then put into standard state space format,

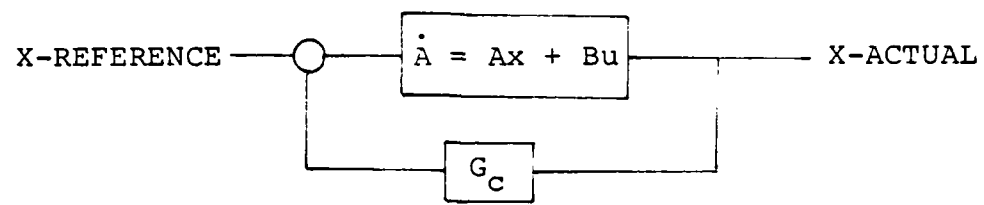
$$\dot{X} = A X + B u \quad (D.8)$$

where $A = M^{-1} F$ and $B = M^{-1} T_1$.

The output equation having C as the identity matrix is,

$$Y = C X$$

Using the mainframe computer CONTROLS program OPTSYS, an optimal controller for the linearized equations of motion is designed and the optimal feedback gain control matrix, G_c , is determined. The closed loop feedback control system for the linearized plant is as follows:



LIST OF REFERENCES

1. Schmitz, E., "Experiments on the End-Point Position Control of a Very Flexible One-Link Manipulator", "Ph.D. Thesis, Stanford Univ., Dept. of Aeronautics and Astronautics, June 1985.
2. Chang, L., "Dynamic Analysis of Robotic Manipulators with Flexible Links", Ph.D. Thesis, Purdue University, Dec 1984.
3. Usoro, P.B., Nadira, R., and Mahil, S.S., "Control of Lightweight Flexible Manipulators: A Feasibility Study", Proceedings, 1984 American Control Conference, Vol. 3, June 1984.
4. Sunada, W.H., and Dubowsky, S., "On the Dynamic Analysis and Behavior of Industrial Robotic Manipulators with Elastic Members", ASME Journal of Mechanisms, Transmissions, and Automation In Design, Vol. 105, pp. 42-51, March 1983.
5. Hastings, G., and Book, W., "Experiments in the Control of a Flexible Robot Arm", Proceedings, ROBOT9 Conference, Vol. 2, RI/SME, pp. 20-45-- 20-27, June 1985.
6. Book, W.J., "Recursive Lagrangian Dynamics of Flexible Manipulator Arms", The International Journal of Robotic Research, Vol. 3, No. 3, Fall, 1984.
7. Cannon, R., and Schmitz, E., "Initial Experiments on the End-Point Control of a Flexible One-Link Robot", The International Journal of Robotic Research, Vol. 3, No. 3, Fall, 1984.
8. Hollars, M.G., and Cannon, R.H., "Initial Experiments on the End-Point Control of a Two-Link Manipulator with Flexible Tendons", ASME Winter Annual Meeting, Miami, Florida, Nov. 1985.
9. Truckenbrodt, A., "Modelling and Control of Flexible Manipulator Structures", Proceedings of 4TH CISM-IFTOMM Symp. on Theory and Practice of Robots and Manipulators, Warsaw, pp. 110-120, 1981.
10. Kelly, F.A., and Huston, R.L., "Modelling of Flexibility Effects in Robot Arms", Proceedings of Joint Automatic Control Conference, Paper No. WP-26, June 1981.

11. MOOG Series 760 Two-Stage Flow Control Servovalve Catalog, MOOG INC., East Aurora, N.Y.
12. Merritt, H.E., Hydraulic Control Systems, Wiley, New York, 1967.
13. Lau, K., Haynes, L. and Hocken, R., "Robot End Point Sensing Using Laser Tracking System", Proceedings, NBS Sponsored-Navy NAV/CIM Robot Standards Workshop, pp.104-111, June 1985.
14. Dunkin, W., "Ultrasonic Position Reference Systems for an Autonomous Sentry Robot and a Robot Manipulator Arm", Masters Thesis, Naval Postgraduate School, Dept. of Electrical Engineering, March 1985.
15. ME Staff Report, "Vision Systems Make Robots More Versatile", Mechanical Engineering, pp. 38-43, Jan 1985.
16. Book, W.J., and Majett, M., "Controller Design for Flexible, Distributed Parameter Mechanical Arms Via Combined State Space and Frequency Domain Techniques", Proceedings, 1982 ASME Winter Annual Meeting, Nov 1982.

INITIAL DISTRIBUTION LIST

	No. Copies
1. Library, Code 0142 Naval Postgraduate School Monterey, California 93943-5000	2
2. Department Chairman, Code 69 Department of Mechanical Engineering Naval Postgraduate School Monterey, California 93943-5000	1
3. Professor Liang-Wey Chang, Code 69 Department of Mechanical Engineering Naval Postgraduate School Monterey, California 93943-5000	1
4. LCDR Robert P. Petroka, USN 504 Fifth Street North Charleroi, Pennsylvania 15022	3
5. Professor David L. Smith, Code 69Sm Department of Mechanical Engineering Naval Postgraduate School Monterey, California 93943-5000	1
6. Professor Robert H. Nunn, Code 69Nn Department of Mechanical Engineering Naval Postgraduate School Monterey, California 93943-5000	1
7. Naval Surface Weapons Center, White Oak Code R402 (ATTN: Mary Lacey) New Hampshire Avenue Silver Spring, Maryland 20910	1
8. LCDR Hobart R. Everett, USN Special Assistant For Robotics, 90G Naval Sea Systems Command Navy Department Washington, D.C. 20362-5101	1

- | | | |
|-----|--------------------------------------|---|
| 9. | Commanding Officer | 1 |
| | Naval Ocean Systems Center | |
| | San Diego, California 92152-5000 | |
| 10. | Defense Technical Information Center | 2 |
| | Cameron Station | |
| | Alexandria, Virginia 22304-6145 | |

END

12-86

DTIC